# STUDY OF THE MAGNETORESISTIVE PROPERTIES OF La$_{n-nx}$Ca$_{1+nx}$Mn$_{n-y}$Cr$_y$O$_{3n+1}$ LAYERED PEROVSKITES

**M. Phil. Thesis**
**(Physics)**

MOHAMMED NAZRUL ISLAM KHAN
Roll No. 040214001P
Session: April 2002

#103163#



**DEPARTMENT OF PHYSICS**
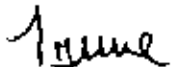**BANGLADESH UNIVERSITY OF ENGINEERING AND TECHNOLOGY (BUET)**
**DHAKA-1000, BANGLADESH.**

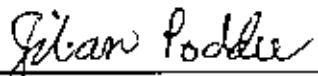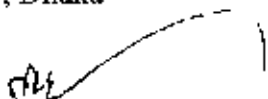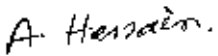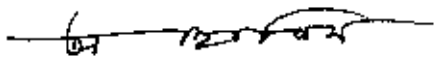# BANGLADESH UNIVERSITY OF ENGINEERING AND TECHNOLOGY
## DHAKA-1000, BANGLADESH

### Certification of Thesis work

The Thesis titled "**STUDY OF THE MAGNETORESISTIVE PROPERTIES OF $La_{n-nx}Ca_{1+nx}Mn_{n-y}Cr_yO_{3n+1}$ LAYERED PEROVSKITES**" Submitted by **MOHAMMED NAZRUL ISLAM KHAN**, Roll No. 040214001P, Registration No. 0402496, Session April-2002 has been accepted as satisfactory in partial fulfillment of the requirement for the degree of **Master of Philosophy (M. Phil)** in Physics on **28 March 2007**.

### BOARD OF EXAMINERS

1. _____      Chairman
   Dr. Mominul Huq (Supervisor)
   Professor, Department of Physics
   BUET, Dhaka

2. _____      Member (Ex-officio)
   Dr. Jiban Podder
   Professor and Head
   Department of Physics
   BUET, Dhaka

3. _____      Member
   Dr. Md. Abu Hashan Bhuiyan
   Professor, Department of Physics
   BUET, Dhaka

4. _____      Member
   Dr. A. K. M. Akther Hossain
   Associate Professor, Department of Physics
   BUET, Dhaka

5. _____      Member (External)
   Dr. A. K. M. Abdul Hakim
   Chief Engineer, Material Science Division
   Atomic Energy Centre, Dhaka

## CANDIDATE'S DECLARATION

It is hereby declared that this thesis or any part of it has not been submitted elsewhere for the award of any degree or diploma.

Date: 28, March, 2007
BUET. DHAKA.

(Mohammed Nazrul Islam Khan)

# Acknowledgements

Date: 28March, 2007

Mohammed Nazrul Islam Khan
Department of Physics
BUET, Dhaka

# Abstract

Bulk layered perovskite samples $La_{n-nx}Ca_{1+nx}Mn_{n-y}Cr_yO_{3n+1}$ ($x = 0.3$; $y = 0.075, 0.15, 0.3$; $n = 2, 3$) were prepared by the conventional solid-state reaction technique. The structure and phase purity of the samples were checked by powder X-ray diffraction (XRD) using Cu $K_\alpha$ radiation ($\lambda = 1.541$ Å) and Phillips (PW3040) X' Pert PRO X-ray diffractometer. The electrical resistivity was measured from room temperature down to liquid nitrogen temperature both in zero field and in an applied magnetic field of 0.7 T. Magnetoresistance (MR) measurements were carried out and the MR behaviour was discussed as a function of magnetic field both at room temperature and at liquid nitrogen temperature. The electrical properties including magnetoresistance of $La_{n-nx}Ca_{1+nx}Mn_{n-y}Cr_yO_{3n+1}$ polycrystals were compared in terms of the number of $MnO_2$ layers and partial substitution of Mn by Cr. In the present investigation it is observed that all the samples showed metal insulator transition with a peak in the electrical resistivity around M-I transition temperature $T_p$. With the increase of Cr doping the resistivity increases but M-I transition temperature $T_p$ decreases. The transport and magnetic properties are sensitively dependent on the number of $MnO_2$ layers, $n$. As the $n$ value decrease from 3 to 2 the transition temperature decreases and the resistivity increases. In the present investigation, it is also observed that the value of resistivity in presence of magnetic field decreases but M-I transition temperature $T_p$ shifts towards the higher temperature region. The transport properties above the transition temperature suggest that conduction mechanism in these manganites is a thermally activated process.

## *Abbreviations*

| | |
|---|---|
| MR | -Magnetoresistance |
| CMR | -Colossal magnetoresistance |
| GMR | -Giant magnetoresistance |
| TMO | -Transition Metal Oxide |
| $T_C$ | -Curie-Wiess transition temperature |
| $T_p$ | -Phase transition temperature |
| $T_N$ | -Neel temperature |
| °C | -Degree centigrade |
| K | -Kelvin |
| eV | -Electron volt |
| $K_B$ | -Boltzman constant |
| GB | -Grain boundary |
| JT | -Jahn-Teller distorn |
| $e_g$ | -Two-fold degenerate state (doublet state) |
| $t_{2g}$ | -Three-fold degenerate state |
| DE | -Double exchange |
| FM | -Ferromagnetism |
| PM | -Paramagnetism |
| AF | -Antiferromagnetism |
| FMM | -Ferromagnetic metal |
| PMM | -Paramagnetic metal |
| TCR | -Temperature coefficient of resistance |
| CFS | -Crystal Field Splitting |
| HTSC | -High temperature Superconductor |
| LFMR | -Low Field Magnetoresistance |
| XRD | -X-ray diffraction |

# CONTENTS

# List of Figures

# List of Tables

# Chapter 1

## Introduction

This thesis deals with the study of the magnetoresistive properties of layered perovskite manganites $La_{n-nx}Ca_{1+nx}Mn_{n-y}Cr_yO_{3n+1}$ (x = 0.3; y = 0.075, 0.15, 0.3; n =2, 3). Rare-earth manganite perovskites of the type $RE_{1-x}AE_xMnO_3$, where RE is a trivalent rare-earth ion and AE is a divalent alkaline-earth ion, have recently been given focus to a large number of experimental and theoretical studies. This is because they exhibit a range of magnetic, electronic, and structural properties including colossal magnetoresistance, charge ordering, magnetic field induced changes in structure, transport properties and also because of potential technological applications.

Although it was observed nearly half a century ago [1-3], there has been keen interest in the past few years when colossal magnetoresistance (CMR) were reported in manganite perovskites $RE_{1-x}AE_xMnO_3$ [4]. Colossal Magnetoresistance is the phenomena of huge changes in electrical resistance upon the application of magnetic field. For manganites the magnetoresistance is very high [5-8] and it is about 99% in the presence of 10T applied magnetic field [9]. The *CMR* effect is achieved only in presence of strong magnetic field (in the tesla range) and in a small temperature window. These classes of materials exhibit different characteristic behaviour depending on the composition, doping agent and oxygen content [10-13]. A small change in the chemical composition like the ratio between trivalent and divalent ions at the A site can induce large change in the physical properties such as structural, magnetic, optical and electronic behaviour. A similar change can occur due to external effect such as magnetic field, a hydrostatic pressure or the temperature.

The $La_{1-x}AE_xMnO_3$ perovskites, where 0.2<x<0.5 and AE=Ca, Sr and Ba etc exhibit a metal-insulator (M-I) transition and ferromagnetic-paramagnetic transition at a certain temperature (100-400 K), depending on the composition, the dopant used and oxygen content. The temperature where the paramagnetic to ferromagnetic transition occurs is known as Curie-Weiss temperature $(T_c)$. Several different studies have shown that $T_c$ and magnetoresistance (MR) near $T_c$ are optimized when x=1/3, i.e. when 33% of the $Mn^{3+}$ is converted to $Mn^{4+}$ (by substituting divalent $A^{2+}$ ions for $La^{3+}$). It was observed that polycrystalline $La_{0.67}A_{0.33}MnO_3$ bulk samples [14,15], thick film [16], thin film [17],

artificial grain boundaries [18-20] and mechanically induced grain boundaries [21] exhibit a low-temperature ($T<<T_c$) low-field MR, in addition to CMR observed around $T_c$. This low-temperature MR is very small in a single crystal or an epitaxial thin film, and is highly sensitive to low -field compared to MR near $T_c$. The coexistence of metallic conductivity and ferromagnetic coupling has been explained in terms of a double exchange (DE) mechanism [22-24]. This mechanism requires a mixed valance state of $Mn^{3+}$ and $Mn^{4+}$ cations in which the $e_g$ electrons from the Mn ions due to a strong Hund's coupling. Though the double exchange (DE) mechanism seems to be a good model, it is not enough to explain all the experimental results. Detailed studies have shown that electron-phonon coupling due to Jahn-Teller effect is also responsible for the observed properties in manganites and a more coherent picture has emerged for the lattice polaron formation associated with the metal-insulator (M-I) transition in these materials {25,26]. There is also a proposition [27] that M-I transition is a consequence of the large to small polaron transition induced by the reduction of effective hopping integrals at temperature near $T_c$. So, to understand the electronic structure of the manganites, one must consider the strong interaction between electrons that form quasi-localized moments, ferromagnetism and antiferromagnetism, canted antiferromagnetism, magnetic ordering, metal-insulator transitions, spin-degrees of freedom, charge and/or orbital ordering effects, polaronic effects, strong electron-phonon conpling and spatial separation of these phases.

Recently, the Ruddlesden-Popper (RP) type layered manganites, $(La-M)_{n+1}Mn_nO_{3n+1}$ have attracted considerable research interest since CMR was observed in the n=2 compounds (M=Ca, Sr)[28]. The RP phases $A_{n+1}B_nO_{3n+1}$, consist of n layers of $BO_6$ corner-sharing octahedra blocks separated by rocksalt AO layers. Apart from the n=1 member, which is an antiferromagnet at any doping concentration, the layered manganites with n=2 and 3 and x = 0.3– 0.4 are found to be ferromagnetic exhibiting CMR effects. Studies of the n=2 compound [29-31] have shown that they have remarkable features including MR ratio enhancement, magnetization, existence of two-dimensional ferromagnetic ordering at a certain temperature range, and the characteristic low-temperature intrinsic MR effect. Recently, it has been reported that the n=3 compound [32-36] exhibits some features that are similar to those observed for the n=2 compound. To date, much of the exploration of the CMR materials has been done through doping of the La sites, which brings about lattice effects, and ultimately influence the double exchange.

Brisi *et al.* [32] reported a tetragonal $Ca_4Mn_3O_{10}$ phase from x-ray powder diffraction analysis, which is considered to have lower symmetry in fact. Henry *et al* [33] studied $Ca_4Mn_3O_{10}$ and $Sr_4Mn_3O_{10}$ and reported that $Ca_4Mn_3O_{10}$ has a space group *Ccc2*. Battle *et al.* [34] determined the structure of $Ca_4Mn_3O_{10}$ and reported a space group *Pbca* according to x-ray and neutron diffraction. A dc magnetization study of $Ca_4Mn_3O_{10}$ was reported by Lago *et al.*[35], and attempts have been made to dope the n=3 member with La in order to induce mixed valence, though only small doping levels have been reported to date in bulk samples. Asano *et al.* [36] reported that the triple layered compound exhibit features that are similar to those observed for the double layered compound.

Asano *et al.* [37] reported that in the perovskite series $La_{n-nx}Ca_{1+nx}Mn_nO_{3n+1}$ (*n*=2, 3, and ∞) thin-film samples with a fixed carrier concentration (x=0.3) have indicated that a reduction in the number of layers results in systematic changes in the various features. These include an increase in resistivity, a decrease in the resistivity peak temperature $T_p$ corresponding to the metal-insulator transition, an enhancement of the maximum MR near $T_p$, and an increase in the low-temperature intrinsic MR.

However, far fewer studies have been conducted in doping the Mn sites. In the last few years, there have been considerable reports on the effects of Mn-site substitution by foreign elements such as Fe, Co, Ni, Al, Ga, Cr etc. Among these doping elements. Cr has a spectacular effect and attracts more attention [38-41].

Barnabe *et al.* [38] showed that among various doping elements, Cr was the most efficient one to induce metal-insulator (MI) transition in $La_{0.5}Ca_{0.5}Mn_{1-x}A_xO_3$. For the Cr doped system, the average *A* site cationic radius is smaller (~1.14 Å) than that of the corresponding undoped system (~1.19 Å). It is well established that antiferromagnetic ordering becomes stronger as cationic radius decreases, so that doping level at the *B* site (here Mn), depending on x, must be increased to counter balance the effect. Moreover as cationic radius decreases, one can see that the range of x values corresponding to ferromagnetic metal (FMM) to paramagnetic insulator (PMI) transition shrinks.

Cabeza and co-researchers [39] studied a Cr doped system, $La_{0.7}Ca_{0.3}Mn_{1-x}Cr_xO_3$. These authors, however, reported no metal-insulator transition for x >0.3 and they also reported very small effect of Cr on the transport property.

Kellel *et al.* [40] studied the magnetoresistive properties of $La_{.7}Sr_{.3}Mn_{1-x}Ti_xO_3$ with x= 0, 0.1, 0.2 & 0.3. They reported that the MI transition temperature decreased when the titanium contents increased.

Maignan *et al.* [41] reported that the doping on Mn site with 5% of Cr in the charge ordered (CO) insulator $Pr_{0.5}Ca_{0.5}MnO_3$ can destroy the charge ordering (CO) antiferromagnetic state and induces an insulator-metal transition.

In this paper the effect of the partial substitution of Mn by Cr on the magnetoresistive properties of the $La_{n-nx}Ca_{1+nx}Mn_{n-y}Cr_yO_{3n+1}$ (x = 0.3; y =0.075, 0.15, 03; n =2, 3) is studied. Like manganese, chromium also exists in two valence states like $Cr^{2+}$ and $Cr^{3+}$. Since the electronic configurations of $Cr^{3+}$ and $Mn^{4+}$ are identical, there is a possibility of substitution of Mn by Cr. In contrast to pseudocubic perovskites the layered versions of $(LaD)_{n+1}Mn_nO_{3n+1}$ consisting of perovskite blocks *n* $MnO_6$ octahedra with an intervening layer of (LaD)O ions might possess various features with different numbers of $MnO_2$ layers, where D stands for divalent ion. Hence the aim of the present investigation is to study the effect of partial substitution of Mn by Cr and variation of the number of layer, n on the magnetoresistive properties of this manganite system.

In this dissertation the preparation, characterization and magnetoresistive properties of the polycrystalline sample $La_{n-nx}Ca_{1+nx}Mn_{n-y}Cr_yO_{3n+1}$ for x = 0.3; y =0.075, 0.15, 03; n =2, 3 are described. The thesis is structured as follows:

**Chapter 2** gives a brief description of the basic issues of CMR in manganites, overview of the properties of CMR materials, intrinsic, extrinsic magnetoresistance, the phase diagrams of various divalent doped manganites, different theoretical model such as double exchange model, Jahn-Teller distortion, etc.

**Chapter 3** describes the details of the sample preparation and experimental techniques used in the present investigation.

**Chapter 4** presents results on magnetoresistive properties of the polycrystalline samples $La_{n-nx}Ca_{1+nx}Mn_{n-y}Cr_yO_{3n+1}$ with the variation of doping and number of layer.

**Chapter 5** summarizes the findings of this dissertation.

## References:

[1] Jonker G H and Van Santen J H, "Ferromagnetic compounds of manganese with perovskite structure", Physica **16**, 337 (1950).

[2] Van Santen J H and Jonker G H, "Electrical conductivity of ferromagnetic compounds of manganese with perovskite structure", Physica **16**, 519 (1950).

[3] Jonker G H and Van Santen J H, "Magnetic compounds with perovskite structure iii. Ferromagnetic compounds of cobalt", Physica **19**, 120 (1953).

[4] Ramirez A P, "Colossal Magnetoresistance", J. Phys. Condens, Matt. **9**, 8171 (1997).

[5] Kusters R M, Singleton J, Keen D A, McGreevy R and Hayes W, "Magnetoresistance measurements of the magnetic semiconductor $Nd_{0.5}Pd_{0.5}MnO_3$", Physica B **155**, 362 (1989).

[6] Tokura Y, Urushibara A, Moritomo Y, Arima T, Asamitsu A, Kido G, and Furukawa N, "Giant magnetotransport phenomena in filling-controlled kondo lattice system: $La_{1-x}Sr_xMnO_3$", J. Phys. Soc. Jpn. **63**, 3931 (1994).

[7] Jin S, Tiefel T H, McCorkmack M, Fastnacht R A, Ramesh R, and Chen J H, "Thousand fold change in resistivity in magnetoresistive La-Ca-Mn-O films", Science **264**, 413 (1994).

[8] Von Helmot R, Wecker J, Holjapfel B, Schultz L, and Samwer K, "Giant negative magnetoresistance in perovskite like $La_{2/3}Ba_{1/3}MnO_3$ ferromagnetic films ", Phys. Rev. Lett. **71**, 2331 (1993).

[9] Akhter Hossain, A K M, Cohen L F, "Influence of grain size on magnetoresistance properties of bulk $La_{0.67}Ca_{0.33}MnO_{3-\delta}$." Journal of Magnetism and Magnetic Materials **192** (2), 263-270 (1999).

[10] Hwang H Y, Cheong S W, Radaelli P G, "Lattice effects on the magnetoresistance in doped $LaMnO_3$," Physical Review Letters **75** (2), 914-917 (1995).

[11] Schiffer P, Ramirez A P, Bao W, "Low Temperature Magnetoresistance and the Magnetic Phase Diagram of $La_{1-x}Ca_xMnO_3$," Physical Review Letters **75** (18), 3336-3339 (1995).

[12] Urushibara A, Moritomo Y, Arima T, "Insulator metal ransition and giant magnetoresistance in $La_{1-x}Sr_xMnO_3$," Physical Review B **51** (20), 14103-14109 (1995).

[13] Rao C N R, Cheetham A K, and Mahesh R, "Giant magnetoresistance and related properties of rare-earth manganites and other oxide systems," Chem. Mater. **8**, 2421-2432 (1996).

[14] Ju H L, Gopalakrishnan J, Peng J L, "Dependence of giant magnetoresistance on oxygen stoichiometry and magnetization in polcrystalline $La_{0.67}Ba_{0.33}MnO_z$," Physical Review B 51 (9), 6143-6146 (1995).

[15] Mahesh R, Mahendiran R, Raychaudhuri A K, "Effect of particle size on the giant magnetoresistance of $La_{0.7}Ca_{0.3}MnO_3$," Applied Physics Letters 68 (16), 2291-2293 (1996).

[16] Akther Hossain A K M, Cohen L F, Berenov A, Macmanus Driscoll J L, "Colossal Magnetoresistance in screen printed $La_{0.67}Ca_{0.33}MnO_3$ thick films", Material Science & Engineering B 77(3), 261-267, (2000).

[17] Shreekala R, Rajeswari M, Ghosh K, "Effect of crystallinity on the magnetoresistance in perovskite manganese oxide thin films," Applied Physics Letters 71 (2), 282-284 (1997).

[18] Mathur N D, Burnell G, Isaac S P, "Large low-field magnetoresistance in $La_{0.7}Ca_{0.3}MnO_3$ induced by artificial grain boundaries," Nature 387, 266-268 (1997).

[19] Steenbeck K, Eick T, Kirsch K, "Influence of a $36.8^0$ grain boundary on the magnetoresistance of $La_{0.8}Sr_{0.2}MnO_{3-\delta}$ single crystal films," Applied Physics Letters 71 (7), 968-970 (1997).

[20] Isaac S P, Mathur N D, Evetts J E, "Magnetoresistance of artificial $La_{0.7}Sr_{0.3}MnO_3$ grain boundaries as a function of misorientation angle," Applied Physics Letters 72 (16), 2038-2040 (1998).

[21] Chatchai Srinitiwarawong and Michael Ziese, "Magnetoresistance of mechanically induced grain boundaries in $La_{0.7}Ca_{0.3}MnO_3$ films," Applied Physics Letters 73 (8), 1140-1142 (1998).

[22] Zener C, "Interaction between d-shels in the transition metals", Phys. Rev. 81, 440 (1951).

[23] Zener C, "Interaction between d-shels in the transition metals. ii. Ferromagnetic compounds of manganese with perovskite structure", Phys. Rev. 82, 403, (1951).

[24] Anderson P W, and Hasewaga H, "Considerations on double exchange", Phys. Rev. 100, 675 (1955).

[25] Zhao G M, Coder K, Keller H, and Müller K A, "Giant oxygen isotope shift in the magnetoresistive perovskite $La_{1-x}Ca_xMnO_{3+y}$ ", Nature, 381, 676 (1996).

[26] Zang J, Bishop A R, and Röder H, "Double degeneracy and Jahn-Teller effects in colossal magnetoresistance perovskites," Phys. Rev. B 53, R8840, (1998).

[27] Srinitiwarawong C, and Ziese M, "Magnetoresistance of mechanically induced grain boundaries in $La_{0.7}Ca_{0.3}MnO_3$ films", Appl. Phys. Lett. 73, 1140 (1998).

[28] Moritomo Y, Asamitsu A, Kuwahara H, and Takura Y, "Giant magnetoresistance manganese oxides with a layered perovskite structure", Nature, (London) 380, 141 (1996).

[29] Asano H, Hayakawa J, and Matsui M, "Magnetoresistance in thin films and bulks of layered-perovskite $La_{2-2x}Ca_{1+2x}Mn_2O_7$", Appl. Phys. Lett. 70, 2303 (1997).

[30] Dörr K, Müller K H, Ruck K , Krabbes G, and Schultz L, "Magnetoresistance of polycrystalline layered manganites $La_{2-2x}Sr_{1+2x}Mn_2O_7$", J. Appl. Phys. 85, 5420 (1999).

[31] Philipp J B, Klein J, Recher C, Walther T, Mader W, Schmid M, Suryanarayanam R, Alff L, and Gross R, "Microstructure and magnetoresistance of epitexial films of the layared perovskite $La_{2-2x}Sr_{1+2x}Mn_2O_7$ (x=0.3 and 0.4)", Phys. Rev. B 65 18441 (2002).

[32] Brisi C and Lucco-Borlera M, Inorg J, "Studies of the $Ca_4Mn_3O_{10}$ structure obtained using high pressure and high temperature" Nucl. Chem. 27, 2129, (1995).

[33] Henry J R, Peter G, Shaun B, Robert H M, Shane J K, Tim J W, Frank J L, and Keith S M, "Ideal n = 3 phase $Ca_4Mn_3O_{10}$ of Ruddlesden–Popper series obtained using high pressure and high temperature" Aust. J. Chem. 49, 205, (1996).

[34] Battle P D, Green M A, Lago J, Millburn J E, Rosseinsky M J, and Vente J F, "Crystal and Magnetic Structures of $Ca_4Mn_3O_{10}$, an n = 3 Ruddlesden-Popper Compound "Chem. Mater. 10, 658, (1998).

[35] Lago J, Battle P D, and Rosseinsky M J, "Weak ferromagnetism and spin-glass behaviour of the n = 3 Ruddlesden-Popper compound $Ca_4Mn_3O_{10}$: a dc magnetization study"J. Phys.: Condens. Matter 12, 2505, (2000).

[36] Asano H, Hayakawa J, and Matsui M, "Magnetotransport in perovskite series $La_{n-nx}Ca_{1+nx}Mn_nO_{3n+1}$ ferromagnets", Appl. Phys. Lett. 71, 844. (1997).

[37] Asano H, Hayakawa J, and Matsui M, "Magnetotransport in perovskite series $La_{n-nx}Ca_{1+nx}Mn_nO_{3n+1}$ ferromagnets", Physical Review B, vol.57(2), (1998).

[38] Barnabe A, Maignan A, Hervieu M, Damay F, Martin C, and Raveau B, Appl. Phys. Lett. 71, 3907 (1997).

[39] O Cabeza, Long M, Severae C, Bari M A, Muirhead C M, Fransisconi M G, and Greaves G, J. Phys.: Condens. Matter 11, 2569 (1999).

[40] Kaltel N, Dezanneau G, Dhahri J, Oumezzin M, Vincent H, "Structure, magnetic and electrical behaviour of $La_{0.7}Sr_{0.3}Mn_{1-x}Ti_xO_3$ with $0<x<0.3$", J magnetism and magnetic materials 261, 56-65 (2003).

[41] Maignan A, Martin C, Damay F, Hervieu M, and Raveau B, "CMR properties of Cr-doped Mn(IV)-rich manganites $Ca_{1-x}Sm_xMnO_3$", J. magnetism and magnetic materials, 188,185 (1998).

# *Chapter 2*

## Literature Review

### 2.1. Introduction

Materials science and engineering have been at the frontier of technological advancement since the bronze and iron ages. The present information age relies on the development of smart and smaller magnetic materials for memories, data storage, processing and probing. These magnetic materials can be divided into numerous categories, depending on their origin and applications. One prime example are the transition metal oxides (TMO) having perovskite ($ABO_3$ type) structure which have been attracting intense attention because of their exotic properties such as ferroelectricity, high temperature superconductivity and colossal magnetoresistance [1,2].

Recently, an approach to electronics is emerging that is based on the up or down spin of the charge carriers rather than on electrons or holes as in traditional semiconductor electronics. Devices that rely on electron's spin to perform their functions form the foundation of spintronics or magnetoelectronics [3-5]. The mixed valence manganites have been studied for more than five decades but are still considered modern materials because of their wide potential for technological application. One of the most interesting properties of the manganites is the influence of a magnetic transition on the electronic conduction. In 1950, Jonker and van Santeen [6-8] discovered that the resistance below the magnetic ordering, the Curie temperature $T_c$ exhibits a positive thermal coefficient, indicating metallic-like behaviour and a negative gradient above $T_c$ based on measurements of polycrystalline ceramics. In 1970, Searle and Wang [9,10] also reported the same behaviour based on single crystals. Despite of much progress, the implications of this behaviour were only explored in 1993, when Chahara *et al.* [11] and von Helmoltz *et al.* [12] reported a reduction of the resistance observed in thin films under the application of an external magnetic field. Herein comes the next generation devices based on Giant Magnetoresistive (GMR) materials. More recently, interest has grown in some materials, specifically $3d$ transition-metal oxides, possess large room-temperature magneto- resistance associated with a paramagnetic-ferromagnetic phase transition whose performance exceeds GMR devices.

In 1994, Jin *et al.* [13] reported that it is possible to reduce the resistivity by several orders of magnitude under the application of very large magnetic field in hole doped manganese oxide perovskites near the Curie temperature $T_c$, which is known as colossal magnetoresistance (CMR). Other compounds such as double perovskites, manganese oxide pyrochlores and europium hexaborides, among others, have presented the same striking property. Thus, research on magnetic materials and understanding its magnetic properties has the potential to make of significant contribution to information technology.

In this review, brief description of the basic issues of CMR in manganites, overview of the properties of CMR materials, intrinsic, extrinsic magnetoresistance, the phase diagrams of various divalent doped manganites, different theoretical model such as double exchange model, Jahn-Teller distortion etc. are presented.

## 2.2. The Phenomenon of Magnetoresistance

Magnetoresistance (MR) refers to the relative change in the electrical resistivity of a material on the application of an external magnetic field. The resistivity of some material is greatly affected when the material is subjected to a magnetic field. This phenomenon is the influence of magnetic transition on the electric conduction. The effect was first discovered by William Thomson in 1857, but he was unable to get lower electrical resistance of anything by more than 5%. But now materials show large magnetoresistance like giant magnetoresistance (GMR), colossal magnetoresistance (CMR) etc.

MR is generally defined by the equation,

$$MR\% = -\frac{\rho(H) - \rho(0)}{\rho(0)} \times 100 \dots\dots\dots\dots\dots\dots\dots (2.1)$$

Where, $\rho(H)$ and $\rho(0)$ are the resistivity at a given temperature in the applied and zero magnetic fields, respectively. MR can be positive or negative depending on the increase or decrease in resistivity, respectively. In non-magnetic pure materials and alloys MR is always positive and MR shows a quadratic dependence on applied magnetic field. MR can be negative in magnetic materials because of the suppression of spin disorder by the magnetic field.

All metals show some MR, but upto only a few percent. Nonmagnetic metals such as Au, exhibit small MR, but the magnitude is somewhat greater (upto 15%) in ferromagnetic metals such as Fe and Co. The semimetal Bi also shows ~ 18% MR in a transverse field of 0.6T, which rises to a 40-fold change at 24T [14]. Cu is more typical in that the same very powerful field (24T) gave rise to change of only ~2% at room temperature. This is the classical positive magnetoresistance that varies as $B^2$ (B = applied magnetic field) in half metallic ferromagnets such as $CrO_2$, $Fe_3O_4$ at low temperature [15]. It is absent in the free electron gas [16] but appears when the fermi surface is non-spherical. This MR originates from the impact of the Lorentz force on the moving charge carriers similar to the Hall effect. Its value is ~ 10% at 10T. A classification of magnetoresistance phenomenon is based on the distinction familiar in magnetism between intrinsic properties such as anisotropy constants, which depend only on the crystal structure, composition and purity, and extrinsic properties of manganites.

### 2.2.1. Giant Magnetoresistance

The Giant Magnetoresistance (GMR) was discovered in 1988 independently by Baibich *et al.* [17] in Paris and Binasch *et al.* [18] in Jülich. It is the phenomenon where the resistance of certain materials drops dramatically as a magnetic field is applied. It is described as Giant since it is a much larger effect than had ever been previously seen in metals. It has generated interest from both physicists and device engineers, as there is both new physics to be investigated and huge technological applications in magnetic recording and sensors.

The GMR effect is most usually seen in magnetic multilayered structures, where two magnetic layers are closely separated by a thin spacer layer of few nm thick. It is analogous to a polarization experiment, where aligned polarizers allow light to pass through, but crossed polarizers do not. The first magnetic layer allows electrons in only one spin state to pass through easily - if the second magnetic layer is aligned then that spin channel can easily pass through the structure, and the resistance is low. If the second magnetic layer is misaligned then spin channel can not get through the structure easily, thus the electrical resistance is high.

11

The GMR effect was originally discovered in Molecular Beam Epitaxy grown epitaxial (100) oriented Fe/Cr/Fe sandwiches [18] and Fe/Cr multilayers [17] but the effects were quite modest at room temperature. Shortly afterwards it was discovered that similar effects could be found in polycrystalline sputtered Fe/Cr multilayers and subsequently very large room temperature MR was found in Co/Cu and related multilayers [19-21]. The GMR has also been observed in variety of inhomogeneous granular systems predominately comprised of Fe, Co, Ni and their various alloys in Cu, Ag and Au matrices [22-24]. In granular magnetic systems, where small ferromagnetic grains are embedded in an immiscible insulating matrix, the macroscopic properties depend on the metallic volume fraction, the grain size and intergranular distance. When the relative orientation of grain is antiparallel, it results in a minimum in conductance. When antiparallel grains are forced to be parallel by the application of a magnetic field, conductance increases and results in large magnetoresistance [25-26]. On the other hand, in magnetic multilayers spin dependent scattering at the interface is responsible for the GMR effect [27].

Grunberg *et al*. (1986) [28] have observed MR in thin film multilayers comprising of two layers of Fe, and Cr layer sandwiched between them. The report of Grunberg went unnoticed by most researchers till Baibich *et al*. (1988) [17], independently observed a drop in resistivity of almost 50% in artificially engineered multilayers by application of external magnetic field and named the phenomenon as Giant Magnetoresistance (GMR). Parkin *et al*. (1995) [29] have found that the relative orientation of the magnetic moments of two neighbouring Co (magnetic) layers depends on the thickness of the intervening spacer Cu (nonmagnetic) layer.

### 2.2.2. Emergence of a New Type of Magnetoresistance: Colossal Magnetoresistance

Another magnetoresistive material which has drawn considerable attention in the last decade are the unique intrinsically layered perovskite ($ABO_3$ type) manganites of the form $RE_{1-x}AE_xMnO_3$, where RE is a trivalent rare earth element e.g. La, Pr, Nd etc. and AE is divalent alkaline earth element e.g. Ca, Ba, Sr etc. Chahara *et al*. (1993) [11], von Helmholtz *et al*. (1993) [12] and Jin *et al*. (1994) [13] observed a high magnetoresistance in these doped rare earth manganites in a magnetic field of several tesla [~6T]. As the physical origin of the magnetoresistance in manganites was completely different from

the Giant Magnetoresistance effect (GMR), and hence the term Colossal was coined to describe the effect.

The initial interest in the potential applications of colossal magnetoresistance was soon prompted by the complexity of the materials. In these materials, the interaction between the electrons and lattice vibrations (phonons) is usually strong, leading to a wide range of striking physical phenomena and most crucially, can be tuned over a wide range by variation of chemical composition, temperature and magnetic field. These materials therefore provide an unprecedented opportunity to study the poorly understood physics of systems in which a high density of electrons is strongly coupled to phonons that demand a microscopic and ultimately atomic characterization of structure, electronic structure and dynamics. The relationships between these structural, electronic, magnetic and optical properties are to be explained in a systematic way.

The research has given rise to important physical concepts, such as double exchange mechanism and the Jahn-Teller polaron, optically and electrically induced magnetic phase transitions, colossal intrinsic magnetoresistance and grain boundary magnetoresistance. The rich electronic phase diagrams reflect the balance of interaction which together determine the electronic ground state. Their properties have been studied for years, both theoretically and experimentally, but a complete understanding remains elusive.

## 2.3. History of Manganites
The mixed-valence manganites perovskite structures have been studied for more than fifty years but are still considered modern materials because of their wide potential for technological applications. In 1950 Jonker and Santen [6-8] described the preparation of polycrystalline samples of $(La,Ca)MnO_3$, $(La,Sr)MnO_3$ and $(La,Ba)MnO_3$ manganites and reported ferromagnetism and anomalies in the conductivity at the Curie temperature with variation in lattice parameter as a function of hole doping. Few years later Volger [30] observed a notable decrease of resistivity for $La_{0.8}Sr_{0.2}MnO_3$ in FM state, in applied magnetic fields. Soon after a significant research effort have started on the studies of low temperature measurement in manganites such as specific heat,

magnetization, dc and ac resistivity, magnetoresistance, magnetostriction, I-V curves, dielectric constant, Seebeck effect and Hall effect [30,31].

After those pioneering experiments, Wollan and Koehler (1955) [32] carried out extensive neutron diffraction study to characterize and draw the first magnetic structures of $La_{1-x}Ca_xMnO_3$ in the entire composition range. They found that in addition to FM phase many other interesting anti-ferromagnetic phases were also present in manganites. Further progress come somewhat later when the group at Manitoba grew a high quality mm long single crystal of another interesting manganites $(La,Pb)MnO_3$, which has a Curie temperature well above room temperature.

Jirak et al. (1979) [33] and Pollert et al. (1982) [34] studied the structure and magnetic properties of another very popular manganites $(Pr,Ca)MnO_3$ by X-ray and neutron diffraction technique. They observed charge-ordering phases which are totally different from the ferromagnetic phases of other manganites.

A burst of research activity on manganites started during 1990 because of the observation of large magnetoresistance. Work by Kusters et al. (1989) [35] on bulk $Nd_{0.5}Pb_{0.5}MnO_3$ reveals the large MR effect. Another work by von Helmholtz et al. (1993) [12] on thin films of $La_{2/3}Ba_{1/3}MnO_3$ also revealed a large MR effect at room temperature. Thereafter similar conclusion was reached by Chahara et al. (1993) [11] using thin films of $La_{3/4}Ca_{1/4}MnO_3$ and Ju et al. (1994) [36] for films of $La_{1-x}Sr_xMnO_3$. They all observed MR values larger than those observed in artificially engineered multilayers (GMR). A defining moment for the field of manganites was the publication by Jin et al. (1993) of results with truly Colossal Magnetoresistance (CMR). Jin et al. [13] reported MR close to 1300% near room temperature and 127,000% at 77K for thin films of $La_{0.67}Ca_{0.33}MnO_3$. This enormous factor corresponds to thousand-fold change in resistivity with and without the field. One year later Xiong et al. (1995) reported MR ratio of over 100,000% using thin films of $Nd_{0.7}Sr_{0.3}MnO_3$ near 60K and in the presence of magnetic field of 8T. These studies led to the obvious conclusion that manganites were a potential alternative for Giant Magnetoresistive systems.

## 2.4. Salient Features of Manganites

### 2.4.1. Electronic Structure of manganites

The parent compound crystallizes in $AMnO_3$ type perovskite structure having general formulas $RE_{1-x}AE_xMnO_3$, where RE stands for trivalent rare earth cation such as La, Pr, Nd, Sm, Eu, Gd, Tb, Y etc. and AE stands for divalent alkaline earth cation such as Ca, Br, Sr etc. In this perovskite like structure (RE,AE) occupies the vertices of the cubic unit cell, Mn occupies the body center and O occupies the six faces of the cube which forms $MnO_6$ octahedra [37-39]. Most manganites from perovskites crystals, including layered perovskites. However, some manganites can be formed of hexagonal layered crystal structures which are different from the cubic structure in atomic view, play some important role resulting different physical characteristics [40].

The perovskite crystal structure can be regarded as a three dimensional network of corner sharing $MnO_6$ octahedra, with Mn ions in the middle of the octahedral. Eight octahedra form a cube, with the A site in its center. In the cubic perovskite, the A-site is twelve-fold surrounded by oxygen ions. But typically the ionic radius of the A ion is similar than the volume enclosed by the oxygen ions. This volume reduced by rotating the octahedra with respect to each other. Inevitably the twelve A-O bond lengths become in equivalent.



(a)          (b)          (c)
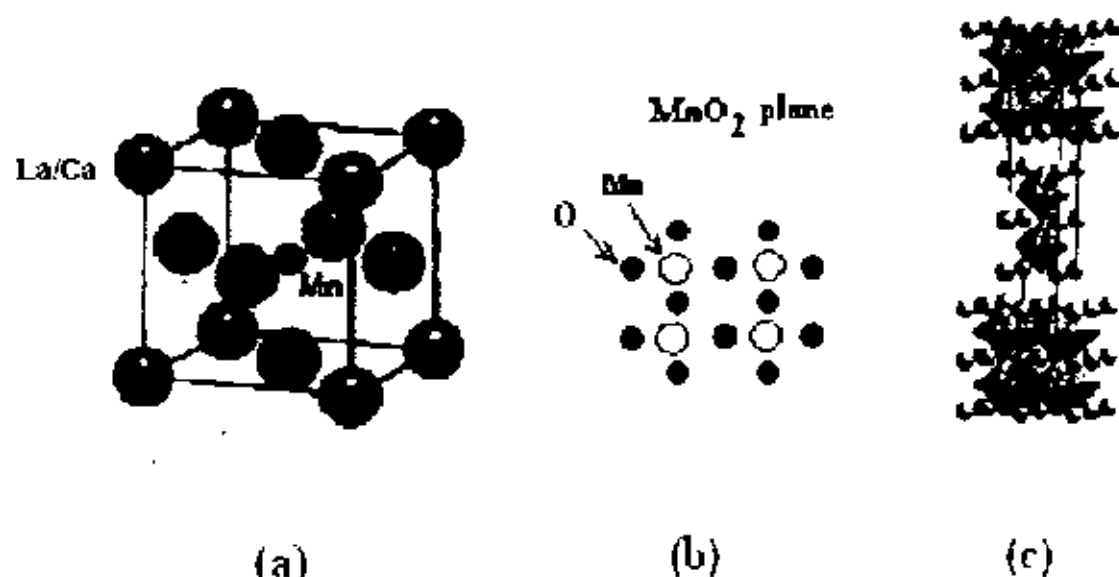
Figure 2.1: Crystal structures of the most important oxides: (a) perovskite structure $(La_{0.7}Ca_{0.3}MnO_3)$; (b) The $MnO_2$ plane, which is identical in the structure to the $CuO_2$ planes of the high temperature superconductors (HTSC's). (c) n = 2 Ruddlesden–Popper phase $(La_{1.2}Ca_{1.8}Mn_2O_7$, $MnO_6$ octahedra are shaded, La/Ca ions are drawn as spheres).

The perovskites crystal structure can be regarded as a three dimensional network of corner sharing $MnO_6$ octahedra, with Mn ions in the middle of the octahedra. Eight octahedra form a cube, with the A site in its centre. In the cubic perovskite, the A site is twelve-fold surrounded by oxygen ions. But typically the ionic radius of the A ion is smaller than the volume, enclosed by the oxygen ions. This volume can be reduced by rotating the octahedra with respect to each other. Inevitably the twelve A-O bond lengths become nonequivalent.

The first report on the crystal structure of the manganites dates back to 1943 by Naray-Szabo [41] and was revised by Yakel [42] in 1955. In contrast to the single cubic unit cell reported by Naray-Szabo, Yakel proposed a monoclinic unit cell, nearly identical to the double cubic cell, but for one angle that is slightly larger than $90^0$. Although the perovskites structure itself was not under discussion, the exact modification was controversial. The $AMnO_3$ has the *Pnma* space group. Just like $LaFeO_3$, $LaMnO_3$ has nearly cubic lattice parameters, which make a structure solution and refinement very hard [43,44]. Elemans *et al.* [45] were the first to report the *Pnma* space group for pure $LaMnO_3$. The oxygen stoichiometry of these $AMnO_3$ compounds is very sensitive to synthesis conditions. Stoichiometric $LaMnO_3$ is an antiferromagnetic insulator with a Neel temperature of 130 $K$ dominated by the strong Coulomb interactions between the electrons. The spins are ordered ferromagnetically in the *ac* plane with the spins parallel to *a*-axis [46]. There is an antiferromagnetic coupling between the layers, along the *b*-axis which is close to $180^0$ [47].

### 2.4.2. Physical overview of doped manganites

The characteristic properties of doped perovskite manganites like the CMR effect and the strong correlation between the structure and electronic-magnetic phases can all be attributed to the ratio of the $Mn^{3+}$ and $Mn^{4+}$ ions. The parent compound crystallizes in $AMnO_3$ type perovskite structure having general formulas $RE_{1-x}AE_xMnO_3$, where RE stands for trivalent rare earth cation such as La, Pr, Nd, Sm, Eu, Gd, Tb, Y etc. and AE stands for divalent alkaline earth cation such as Ca, Br, Sr etc. In this perovskite like structure (RE,AE) occupies the vertices of the cubic unit cell, Mn occupies the body center and O occupies the six faces of the cube which forms $MnO_6$ octahedra. The (RE,AE) site can in most cases form homogenous solid solution. Both the end members

LaMnO$_3$ and CaMnO$_3$ are antiferromagnetic insulator having single valent Mn ions i.e. Mn$^{3+}$ and Mn$^{4+}$ respectively. On partial doping of the trivalent RE-ion by divalent alkaline earth cation AE, leads to the formation of a mixed valence state of the Mn i.e. Mn$^{3+}$ and Mn$^{4+}$ to maintain the charge neutrality of the system. The mixed valency of the Mn ions may also be controlled by varying the oxygen content. This doping with some divalent cation causes the structure to get distorted due to the differences in the size of the various atoms and leads to Jahn-Teller effect. Perovskite-based structures occasionally show lattice distortion as modifications from the cubic structure due to doping. One of the possible origin in the lattice distortion is the deformation of the MnO$_6$ octahedron arising from the Jahn-Teller effect that is inherent to high-spin (S=2) Mn$^{3+}$ with double degeneracy of e$_g$ orbital. Another lattice deformation comes from the connection pattern of the MnO$_6$ octahedra in the perovskite structure, forming rhombohedral or orthorhombic lattices. In these distorted perovskites, the MnO$_6$ octahedra show alternate buckling. Such a lattice distortion of the perovskite AMnO$_3$ (where A=RE$_{1-x}$AE$_x$) is governed by the Goldsmith tolerance factor 't' which measures the deviation from perfect cubic symmetry (t=1) and is defined as,

$$t = (r_D + r_O)/\sqrt{2}(r_T + r_O) = 1 \quad \dots\dots\dots\dots\dots (2.2)$$

where $r_D$, $r_T$ and $r_O$ are the radii of the divalent, trivalent, and oxygen ions, respectively [5]. The tolerance factor measures the deviation from perfect cubic structure (t=1). By using mixtures of T= La, Pr, and Nd and D =Ca, Sr, Ba, and Pb, t can be varied, with the result that the perovskite structure is stable for 0.85< t <0.91. At finite doping, charge balance is maintained by a fraction, x, of Mn ions assuming a tetravalent, Mn$^{4+}$ (d$^3$), configuration in a random fashion throughout the crystal, with the remainder in the Mn$^{3+}$(d$^4$) state presumably, D substitution is equivalent to hole doping, but thermo power and Hall effect disagree on the carrier sign in the paramagnetic state, suggesting that a simple band picture is not valid. Mixed valency can also be modified by varying the oxygen content. For x=0 and 1, M (T< 100K) was found to be small, indicating an antiferromagnetic (AF) ground state.

At intermediate values of x, M rises and peaks with its Hund's-rule value at x=0.3. In subsequent work van Santen and Jonker showed that at temperatures above the ferromagnetic Curie point, $T_c$, the resistivity behaves like a semiconductor, $d\rho/dT<0$, but

that below $T_c$, not only is there a sharp reduction in resistivity, but also a transition to metallic behaviour, $d\rho/dT > 0$ [6]. This behaviour is shown for $La_{1-x}Sr_xMnO_3$ and $La_{1-x}Ca_xMnO_3$ in figures 2.2 and 2.3.
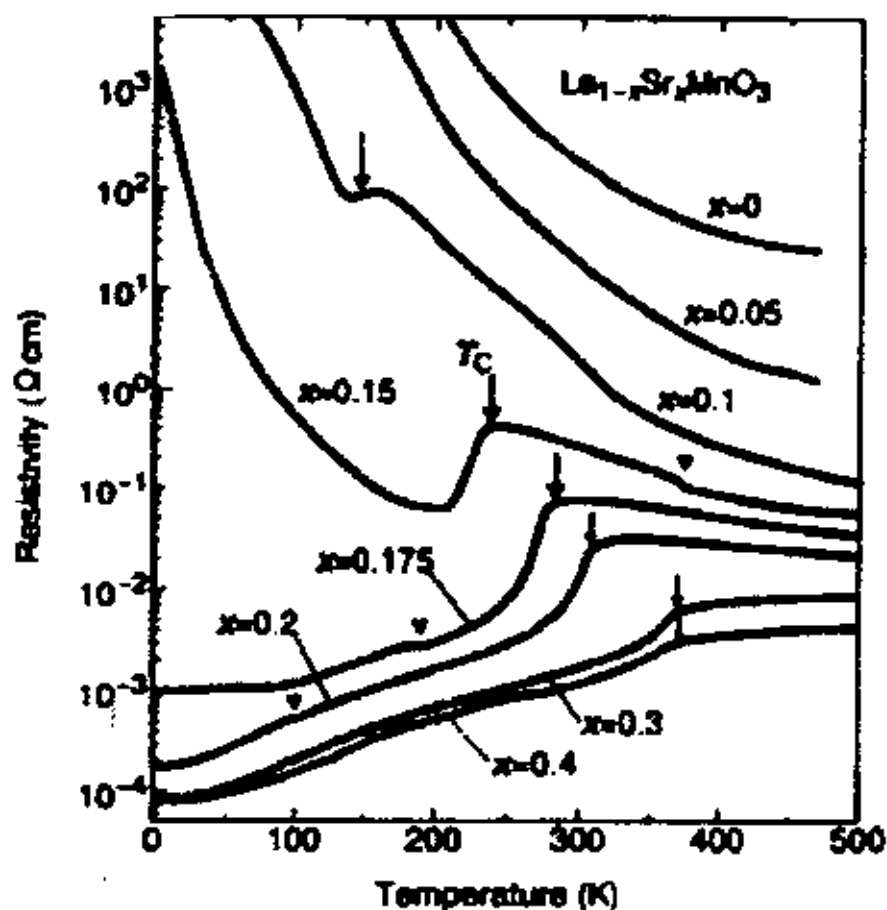


Figure 2.2: Resistivity against Temperature for $La_{1-x}Sr_xMnO_3$ for various x values. The arrows denote the transition as determined by magnetization measurement [73].
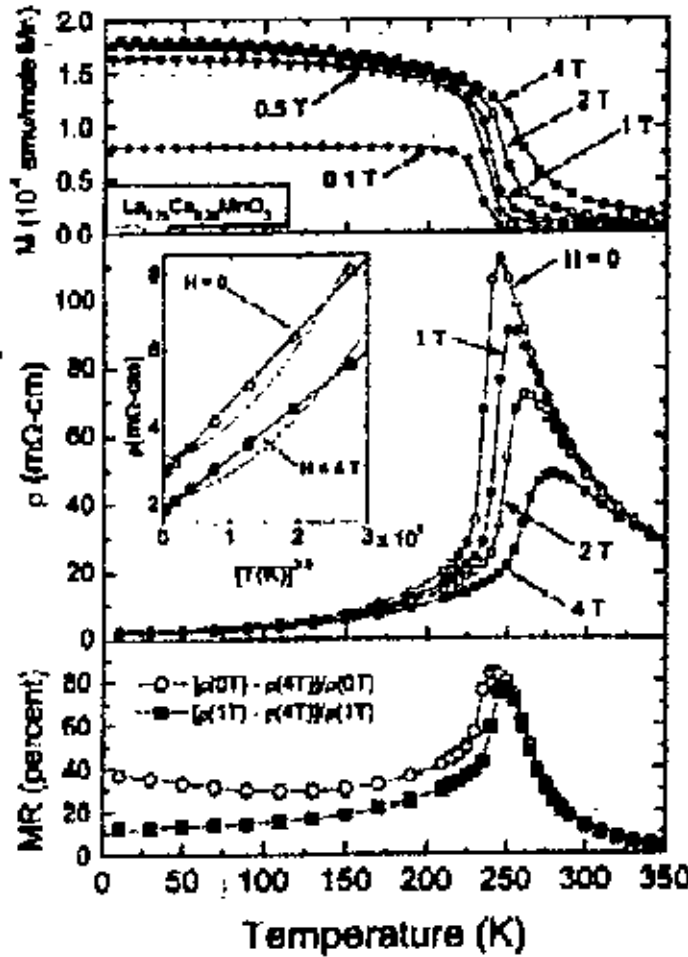
Figure2.3: Top frame- magnetization against temperature for $La_{0.75}Ca_{0.25}MnO_3$ for varies field values. Middle frame resistivity against temperature The inset shows the low temperature resistivity compared to $T^{2.5}$ (solid line) and $T^{4.5}$ (dashed line) behaviour. Bottom frame-magnetoresistance against temperature. Open symbols reflect low-field behaviour and solid symbols reflect the high field behaviour.

### 2.4.3. Ionic view of electronic structure

Fig. 2.4 shows the electronic configuration for the $Mn^{3+}$ and $Mn^{4+}$ ions in the compound $AMnO_3$ in a hybrid orbital structure. Mn ions have an incomplete $d$-shell (Mn: [Ar] $3d^64s^2$). According to the Hund's rule, in ordr to minimize the energy, all the unpaired electrons in outer $d$-shell align their spins parallel to one another. Thus only five $d$-levels corresponding to the majority spin are accessible.
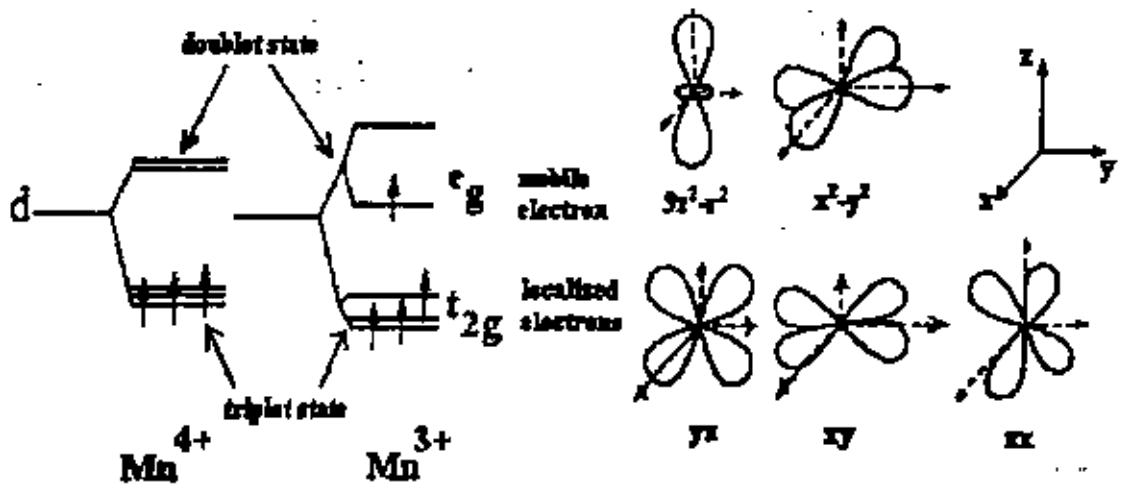
Figure 2.4: Electron states of the outermost $3d$ energy level of the $Mn^{3+}$ and $Mn^{4+}$ ions.

Hund's rule is implied by two interaction: Coulomb repulsion makes electrons to be in different d-orbital each; Hund's coupling obliges the electron spins to be parallel. In isolated atoms, the five $d$ levels are split into three-fold degenerate $t_{2g}$ ($d_{xy}$, $d_{yz}$ and $d_{zx}$) and two-fold degenerate $e_g$ ($d_{x^2-y^2}$ and $d_{3z^2-r^2}$) due to the cubic symmetry in which manganites crystallize [48]. The $t_{2g}$ orbitals are lower in energy than the $e_g$ orbitals because the later are aligned with the p-oxygen levels leading to a larger Coulomb repulsion than in other directions. $Mn^{4+}$ has three electrons in the outer $d$-shell that can be considered as localized in the three $t_{2g}$ levels giving a total spin S=3/2. The two $e_g$ levels remain empty. On the other hand $Mn^{3+}$ has an extra electron that fills one of the $e_g$ level, which spin S=2. This single electron is unstable, hence the system reduces its energy by splitting the double state into two hyperfine energy levels. This well-known phenomenon is called the Jahn-Teller effect [49]. These $e_g$ levels are the active ones for conductivity. These levels hybridize with oxygen p-levels [50] consisting the conduction band whose bandwidth depends on the overlapping of the $e_g$ orbital of the Mn and the p-levels of the oxygen. The minority anti-parallel spin levels are very high in energy. This implies that only the majority spins can conduct. For this reason, manganites are called half-metals.

Fig-2.5 outlined the electronic hopping within narrow and fully spin-polarized bands are supported by a band structure calculation made for the end members of one dilution series, $LaMnO_3$ and $CaMnO_3$ [51]. For $LaMnO_3$ this calculation shows a typical

separation between up and down polarized bands of about 1.5 eV and bandwidths of order 1-1.5 eV. Photoemission experiments on $La_{1-x}D_xMnO_3$ (D= Ca, Pb) confirm these basic features [52]. The density of states for such a system is shown schematically in the figure. It has shown for comparison is the density of states for Ni metal. Since the up and down spin bands are well separated, the magnetic polarization (saturation moment) is 100%, compared to 11% in Ni. This will lead to reversal of carrier spin direction across FM domains and large grain-boundary effects.
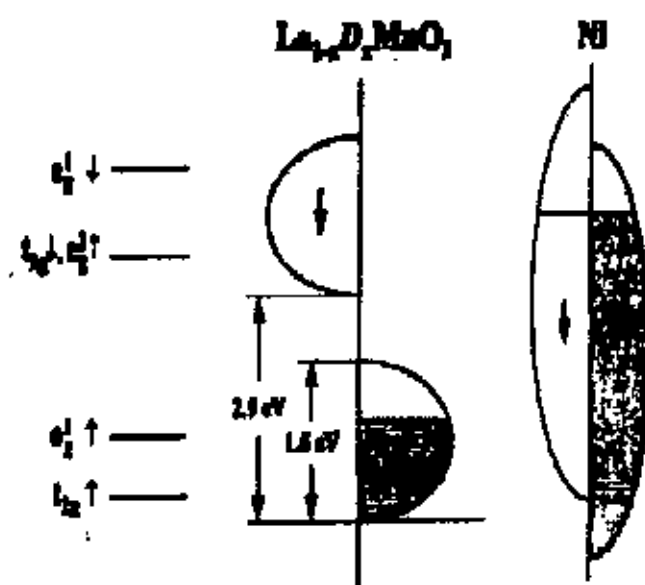


**Figure 2.5:** Schematic T=0 density of states for doped $LaMnO_3$ The level diagram to the left shows the approximate positions of the 3d bands in undoped $LaMnO_3$. The energy scale for $La_{2/3}Sr_{1/3}MnO_3$ is extracted from photoemission data. Comparison is made to Ni metal which possesses a much smaller degree of spin polarization.

### 2.4.4. Layered manganese oxide perovskites

Manganese is three-dimensional perovskites. The perovskite structure consists on a lattice of oxygen octahedra with a Mn ion in their center, where the trivalent $La^{3+}$ site is substituted by divalent $Ca^{2+}$ ion. Therefore, there is an oxygen ion between every two manganese as shown in the $MnO_2$ plane. The structure of these planes is completely analogous to the $CuO_2$ planes found in the cuprate high temperature superconductors (HTSC's). The $MnO_2$ planes are then stacked in a variety of sequence with $MnO_2$ planes interleaved with (La, Ca)O planes in figure 2.6.

$MnO_6$
Octaheda

■ A atom
(La-Ca)

c

a

n = ∞          n = 3          n = 2
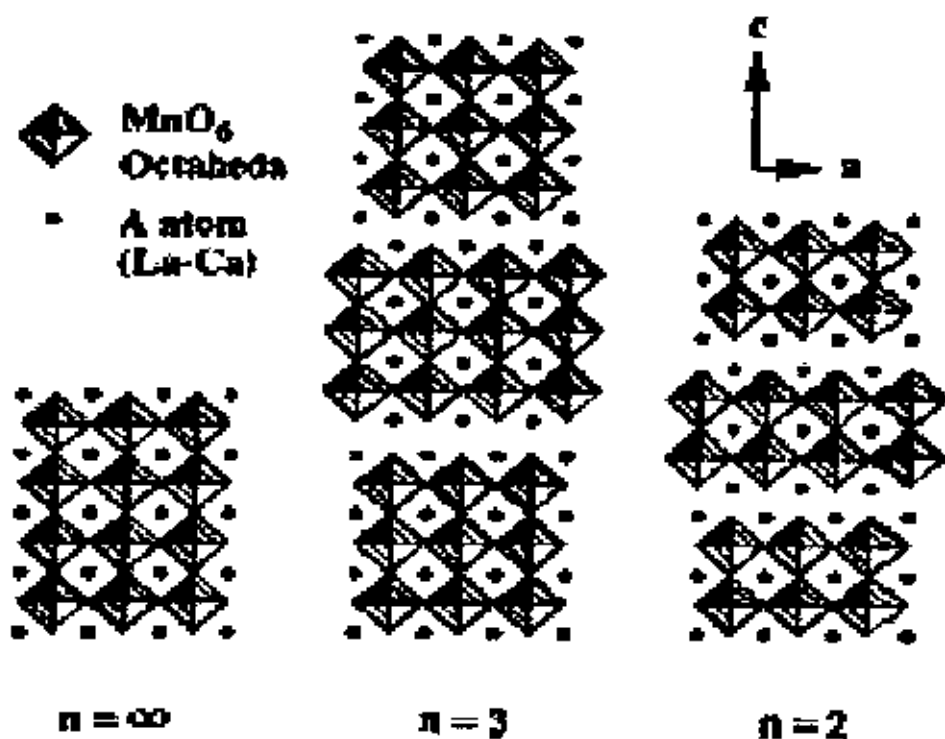
**Figure 2.6**: The crystal structure of the layered manganites.

The compounds are annotated depending upon how many $MnO_2$ planes are arranged between the bi-layer of (La, Ca)O planes. La and Ca can be replaced by many other trivalent and divalent ions. This series is called the Ruddlesden-Popper (RP) series, and has the general formula $(La, Ca)_{n+1}Mn_nO_{3n+1}$. The n = 1 compounds have formula unit $(La,Ca)_2MnO_4$ and are analogous to the HTSC compounds $(La, Ca)_2CuO_4$. The n = 2 compounds have the formula unit $(La,Ca)_3Mn_2O_7$ and n=3 have $(La,Ca)_4Mn_3O_{10}$. The n = ∞ compounds have no (La,Ca)O bilayers, and have the formula unit $(La,Ca)MnO_3$. They are cubic or distorted cubic compounds, and the most heavily studied of the manganites. The layered compounds (n ≠ ∞) cleave much more readily than the cubic compounds and so are more suitable for the spectroscopic measurements [53].

## 2.4.5. Transport properties of CMR materials

In magnetism, it is customary to distinguish an intrinsic property, which depends only on the bulk chemical composition and crystal structure, from extrinsic properties that are governed by the sample size and microstructure. For example, hysteresis is generally an extrinsic property, where as on the other hand, spontaneous magnetization is an intrinsic property. Intrinsic properties are best measured on single crystal and epitexial film. Magnetoresistance can be an intrinsic or an extrinsic property. Intrinsic magnetoresistance is maximum close to the ferro-paramagnetic transition and appears due to the intrinsic interactions in the materials. The general form of the magnetization and the resistivity of CMR materials are shown in figure 2.7.
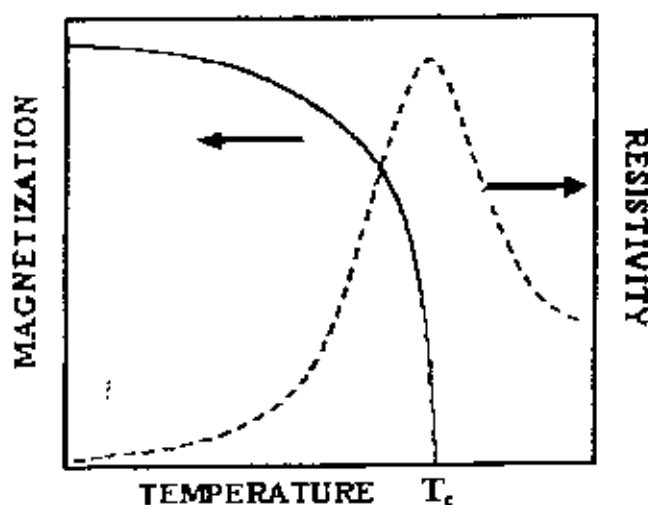


**Figure 2.7**: Resistivity and magnetization as a function of temperature.

When a magnetic field is applied, the peak on the resistivity moves toward higher temperature and dramatically decreases its height. As shown there the magnetic transition is accompanied by a change in the behaviour of the resistivity with temperature. The system is metallic below the magnetic critical temperature $T_c$ ($d\rho/dt > 0$) and insulator in the paramagnetic region ($d\rho/dt < 0$). $T_c$ ranges from the $15K$ for $EuB_6$ to more than $500\ K$ for double perovskites. In particular, manganites cover a wide range of $T_c$ (100-400K). Approaching $T_c$ from below, the resistivity increases dramatically-sometimes by order of magnitude.

23

The polycrystalline samples show a completely different behaviour characterized by two futures: a sharp increase of magnetoresistance at low field and at linear background at higher-fields. It has been suggested by Gupta et al. [54], and Li et al. [55] that the low-field magnetoresistance, which is consistently observed in polycrystalline manganites, is due to spin-dependent scattering in grain boundaries. A low external field can readily rotate the grain magnetization into a parallel configuration and thereby cause a significant drop in resistivity and low-field magnetoresistance. The degree of spin polarization is temperature dependent and increase with decreasing temperature [56]. Hwang et al.[57] suggested that the effect was due to spin-dependent tunneling between adjacent grains separated by an insulating grain boundary constituting a tunnel barrier for the spin-polarized conduction electrons. Also within this model the low-field magnetoresistance can be explained by the alignment of magnetizations of neighboring grains.

Spin-dependent scattering or spin-dependent tunneling can explain the low-field magnetoresistance but fail to explain the linear high-field magnetoresistance. Evetts et al. [58] suggested that the high-field magnetoresistance is associated with a magnetically mesoscopic disordered interface layer present in the vicinity of grain boundaries. The transport mechanism in the interface layer is the same as in the bulk parts of the grains, but the layer has depressed Curie temperature and magnetization, which could be caused by strain, defects and weakened or absent bonds near the grain surface. The high-field MR could be related to alignment of spins in the disordered interface layer.

### 2.4.6. Transport properties of few other polycrystalline materials

The effects of grain boundaries on the resistivity and magnetoresistance of polycrystalline manganites compounds were reported very early by Volger et al. [30]. The recent research was initiated by the work of Hwang et al.[57] and Gupta et al.[54]. These authors compared the magnetoresistance and the magnetization of $La_{0.67}Sr_{0.33}MnO_3$ single crystals and polycrystalline ceramics and $La_{0.67}Ca_{0.33}MnO_3$ and $La_{0.67}Sr_{0.33}MnO_3$ epitaxial and polycrystalline films respectively. Both investigations found that the resistivity and magnetoresistance depends sensitively on the microstructure, whereas the magnetization was hardly affected.
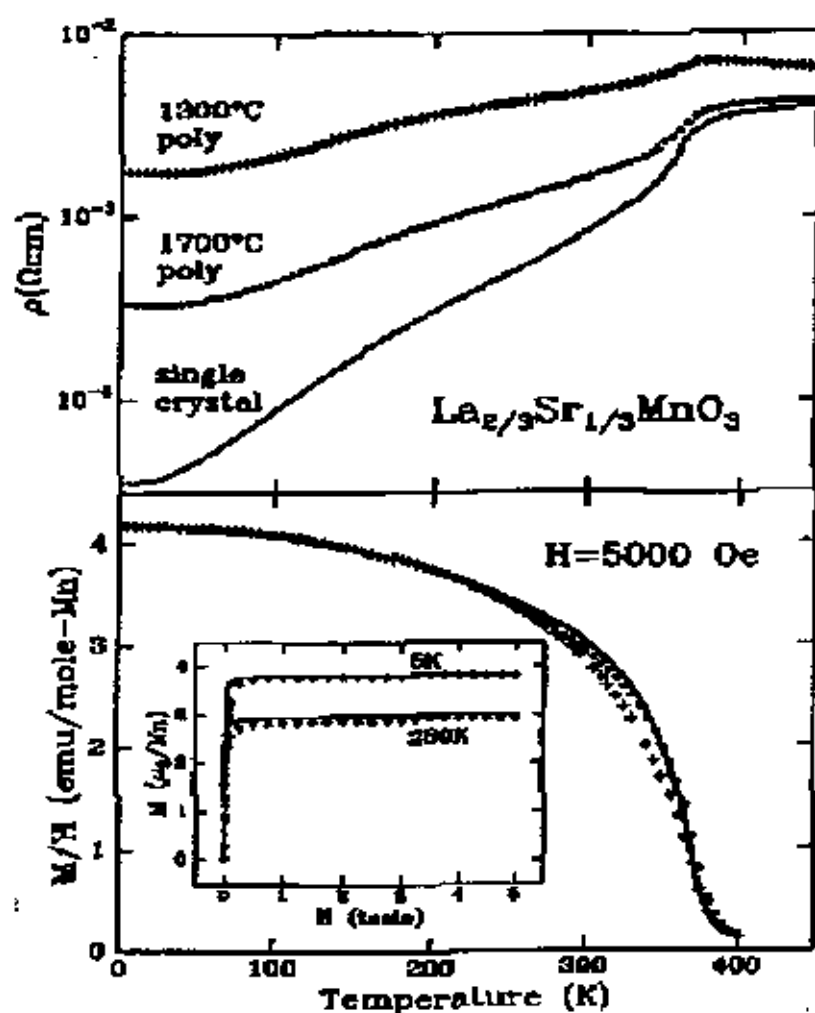
**Figure 2.8:** Top panel: zero-field resistivity of $La_{0.67}Sr_{0.33}MnO_3$ single crystal and polycrystals as a function of temperature. Bottom panel: magnetization of the sample as a function of temperature measured at B=0.5 T. The inset shows the field-dependent magnetization at 5 and 280 K reproduced from Hwang *et al.*[57]
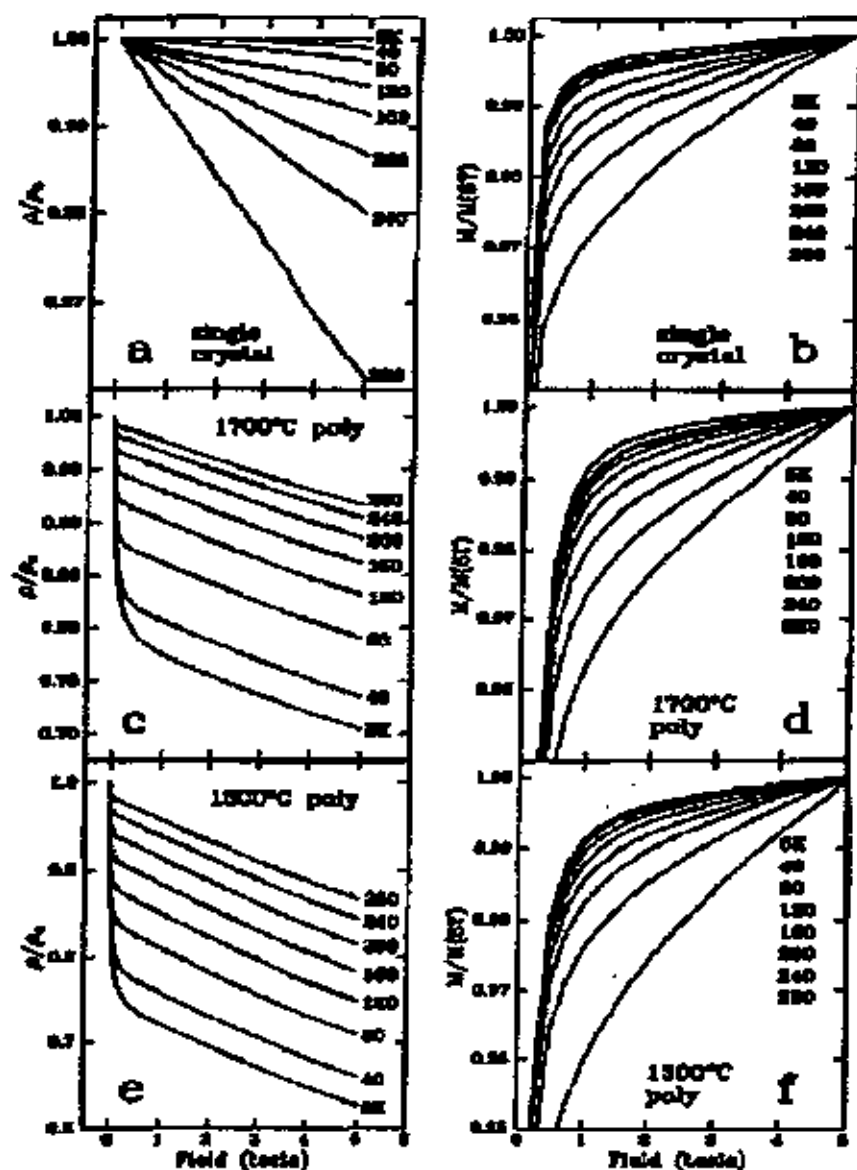
**Figure 2.9:** Magnetoresistance data of the samples. Panels (*a*), (*c*) and (*e*): normalized resistivity $\rho/\rho_0$ as a function of magnetic field. $\rho_0$ denotes the zero-field resistivity. Panels (*b*), (*d*) and (*f*): magnetic field dependence of the normalized magnetization reproduced from Hwang *et al.*[57]

Figure 2.8 shows the zero-field resistivity and the magnetization of the samples as a function of temperature. Whereas the low-temperature resistivity depends strongly on the microstructure, the magnetization of the three samples is virtually identical. The effect of the grain boundaries on the magnetoresistance is more dramatic. Figure 2.9 shows the field dependent resistivity and magnetization of the samples. The single crystal shows the magnetoresistance linear in magnetic field. The polycrystalline samples show a sharp drop at low magnetic field followed by a linear dependence at higher fields. Again the field dependence of the magnetization is virtually identical for the three samples. The magnitude of the low-field magnetoresistance increases with decreasing temperature in contrast to the intrinsic magnetoresistance that has a maximum value near the Curie temperature and decreases with decreasing temperature. These results cannot be explained by the intrinsic magnetoresistance alone, since the intrinsic magnetoresistance is only a function of the magnetization. Hwang *et al.* suggested that the low-field magnetoresistance in polycrystalline samples is due to spin polarized tunneling between the misaligned grains.

### 2.4.7. Intrinsic and Extrinsic magnetoresistance

Magnetoresistance can be intrinsic or extrinsic in property. In this section the intrinsic and extrinsic magnetoresistance is discussed and also illustrate how they can be distinguished from experiment. Some results from the literature are used for exemplification.

### Intrinsic Magnetoresistance

. Intrinsic magnetoresistance is closer to the ferromagnetic-paramagnetic transition and appears due to the intrinsic interactions in the materials. Figure 2.10 shows the temperature dependence of the zero field and $\mu_0=5T$ resistivities of a single-crystalline thin film $La_{0.7}Ca_{0.3}MnO_3$ sample, data obtained from Hundley *et al.* [59]. The corresponding magnetoresistance is shown in the same graph. This sample has no internal grain boundaries so the magnetoresistive response is therefore entirely intrinsic.
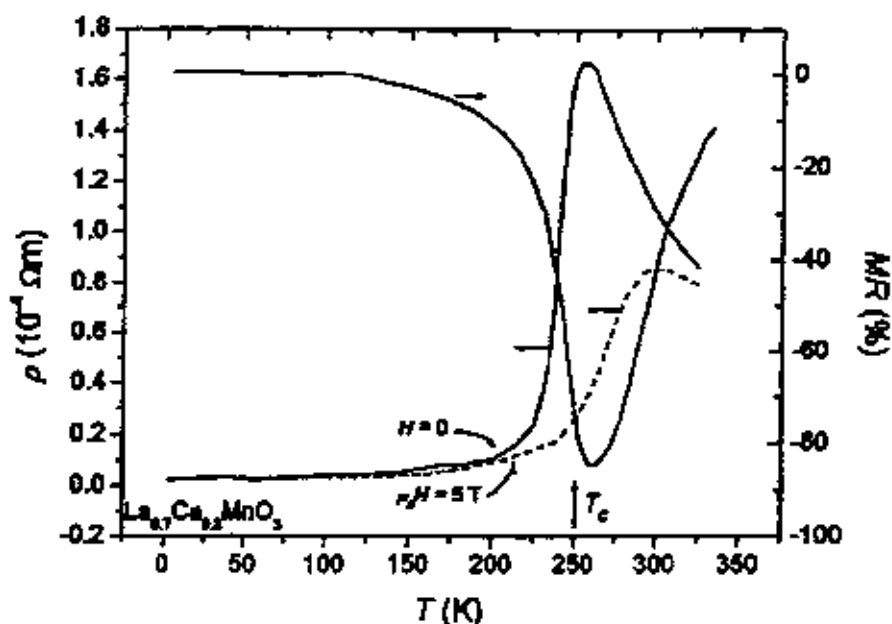
**Figure 2.10:** Resistivity of single-crystalline thin-film $La_{0.7}Ca_{0.3}MnO_3$ in zero magnetic field and in an applied field of 5T. The graph shows also the corresponding Magnetoresistance adopted from Hundly et al.[59]

The thin-film substance shows a metal-insulator transition coinciding with the ferromagnetic-paramagnetic transition at the temperature (250 K). Qualitatively, the temperature dependence of the magnetoresistance can be explained in terms of Zener's double-exchange mechanism. The simplest expression for conductivity is $\sigma = ne\mu$, where n is the number of carries, e is their charge, and $\mu$ their mobility. The metal-insulator transition could thus originate from either a change of the number of carriers or a change the mobility of the carriers. In the double-exchange theory the change of hopping mobility is the dominant effect on the conductivity .The transfer integral for electron transport between adjacent Mn sites is $t=t_0\cos(\theta/2)$ where $\theta$ is the angle between the spin directions of the two Mn cores spins. Below the ferromagnetic transition temperature the spin system is ferromagnetically ordered and the probability for electron transfer (and thereby the mobility) is high. The zero-field resistivity shows metallic-like temperature dependence with a positive slope. Around the Curie temperature the spin system becomes disordered because the thermal energy exceeds the ferromagnetic exchange energy. The hopping amplitude decreases and a drastic increase of the zero-field

28

resistivity is observed. Above $T_c$ the resistivity decrease with temperature as expected for an insulator, where transport is thermally activated. The sample exhibits a large negative magnetoresistance peaking just above the Curie temperature. Below $T_c$ the spins align spontaneously and the external field has little influence on $\theta$. The magnetoresistance gradually vanishes when the magnetic moment approaches its saturation value. Near $T_c$, however, the spin system is highly susceptible to the external field, which causes a substantial change of the local spin disorder and thereby of the carrier mobility. Thus, the field drives the material more metallic. Far above the Curie point the external field can no longer compete with the thermally induced random spin fluctuations and the magnetoresistive response decreases with temperature.

Many research groups have suggested that double exchange alone is not sufficient in order to explain the CMR. The models proposed evoke a competition between double exchange and another mechanism-such as polaron formation due to the strong electron-phonon coupling or localization by spin fluctuations; this competition is supposed to drive the metal-insulator transition. The balance between the two competing mechanisms is very sensitive to an applied magnetic field that suppresses spin fluctuations and enhances the ferromagnetic order. The debate on the essential transport mechanism in the manganites has not yet been decided.

It has been also suggested by Coey *et al.* [60] or Von Helmolt *et al.* [61] that the very large change in resistivity observed for manganites is due to magnetic polaron formation in the paramagnetic regime. The $e_g$ electrons may induce a local polarization of its neighboring spins forming a small ferromagnetic entity called a magnetic polaron. According to their suggestion a magnetic polaron can be considered a quasi-particle and it can jump from lattice site to lattice site carrying along its spin polarization. This hopping takes place via thermal activation. Below the curie temperature (or when a magnetic field is applied) the magnetic polarons are destroyed. This could contribute to the abrupt change of resistivity near $T_c$. Another kind of polarons, which could be present in manganites, are dielectric polarons formed due to the coulomb interaction between the electron and its surrounding ionic charges. The concept of polaron transport in mixed-valence manganites is not yet fully understood.

In theoretical results by Millis *et al.* [62] the resistivity was obtained from a dynamical mean-field calculation including double exchange and a coupling of carriers to phonons. The calculations show that the resistivity above $T_c$ can be tuned from semiconducting to metallic on decrease of the electron-phonon coupling strength.

**Extrinsic Magnetoresistance**

Figure 2.11(a) compares the temperature dependence of magnetoresistance of a single-crystalline manganite (an epitaxial thin film) with that of a polycrystalline thin film having the same composition $La_{0.67}Ca_{0.33}MnO_3$. Data was obtained from Gupta *et al.*[54]. Both samples show a magnetoresistance maximum near the Curie temperature, which can be ascribed to intrinsic magnetotransport (the CMR effect). For the epitaxial film the magnetoresistance vanishes at low temperatures, as expected for a single-crystalline material. However, the polycrystalline film shows an increasing magnetoresistance with decreasing temperature.

Figure 2.11(b) shows the field dependence of magnetoresistance at two different temperatures below the ferromagnetic transition temperature. The epitaxial sample shows a linear variation of the magnetoresistance with the applied field. This indicates that the Bloch wall motion and rotation in single-crystalline manganites do not dominate transport. The magnetoresistance varies smoothly through the region of domain rotation, which takes place in low fields, so the increasing magnetoresistance is mainly due to enhance magnetic order. The magnetoresistance effect is small and decreases with decreasing temperature. The polycrystalline sample exhibits a completely different behavior characterized by two features: 1) a sharp increase of magnetoresistance at low-fields followed by 2) at linear background at higher fields. The slope of the high field contribution is broadly temperature independent. The low-field magnetoresistance, which is often termed LFMR, increases with decreasing temperature.

It has been suggested by Gupta *et al.* [54], and Li *et al.* |55| that the low-field magnetoresistance, which is consistently observed in polycrystalline manganites, is due to spin-dependent scattering in grain boundaries. In ferromagnetic metals the exchange energy splits the conduction band into majority and minority carrier bands resulting in a spin imbalance at the Fermi level. In mixed-valance manganites the majority and the minority bands are separated by an energy gap arising from the strong intra-atomic

30

coupling between the 3d $e_g$ conduction electrons and the 3d $t_{2g}$ core spins [63]. The spin polarization may therefore approach 100% at low temperatures (thus, manganites may be characterized as half-metals). In the ferromagnetic state each grain in a polycrystalline manganite may constitute a single magnetic domain.

In the virgin state, where no field is applied, the grains have their magnetic moments randomly oriented. The polarized conduction electrons are easily transferred between Mn sites within a magnetic domain. However, an electron traveling across a grain boundary to an adjacent grain (or domain) may become subject to a strong spin dependent scattering leading to a high zero-field resistivity. A low external field can readily rotate the grain magnetization into a parallel configuration and thereby cause a significant drop in resistivity and low-field magnetoresistance. The degree of spin polarization is temperature dependent and increases with decreasing temperature [56].
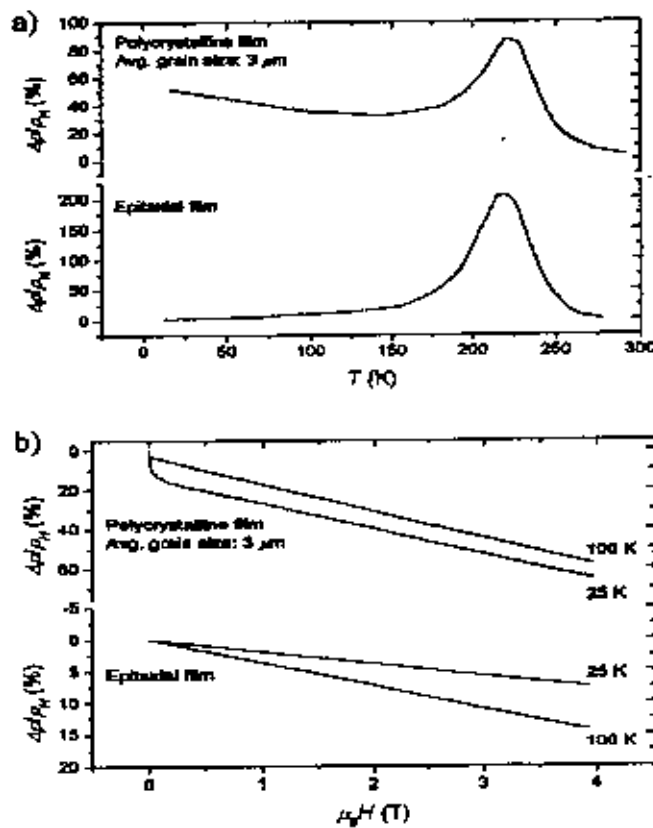


**Fig 2.11:** Magnetoresistance for a field change of 0 to 2 T versus temperature of poly-crystalline (top panel) and epitaxial (bottom panel) thin film $La_{0.67}Ca_{0.33}MnO_3$.b) Magnetoresistance as a function of applied field taken at 25 and 100 K.

This could explain why the low-field magnetoresistance becomes more and more dominant as the temperature is decreased. Spin-dependent scattering of polarized conduction carriers is the dominant mechanism describing spin-valve effects in metallic GMR multilayers [64].

Hwang *et al.* [57] offered a different explanation to the low-field magnetoresistance effect observed below the Curie temperature. The compared the magnetoresistive properties of single-crystalline and polycrystalline $La_{0.67}Sr_{0.33}MnO_3$ and also observed LFMR (low field magnetoresistance) in the polycrystalline samples, which was absent in the single crystal. They suggested that the effect was due to spin-dependent tunneling between adjacent grains separated by an insulating grain boundary constituting a tunnel barrier for the spin-polarized conduction electrons. Also within this model the low-field magnetoresistance can be explained by the alignment of magnetizations of neighboring grains.

Spin-dependent scattering or spin-dependent tunneling can explain the low-field magnetoresistance but fail to explain the linear high-field magnetoresistance. Evetts *et al.*[58] suggested that the high-field magnetoresistance is associated with a magnetically mesoscopic disordered interface layer present in the vicinity of grain boundaries (fig 2.12). The transport mechanism in the interface layer is the same as in the bulk parts of the grains, but the layer has depressed Curie temperature and magnetization, which could be caused by strain, defects and weakened or absent bonds near the grain surface. The high-field MR could be related to alignment of spins in the disordered inter-face layer.
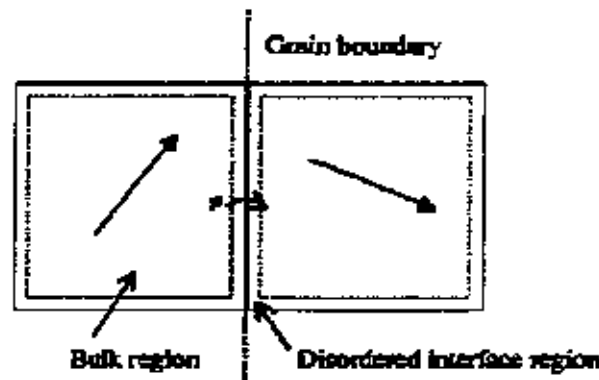


**Figure 2.12:** Schematic illustration of grain-boundary transport in a polycrystalline mixed-valence manganite.

Figure 2.12: Schematic illustration of grain-boundary transport in a polycrystalline mixed-valence manganite. Each grain constitutes a single magnetic domain. The conduction electrons show a high degree of spin polarization inside the grains. When traveling across the grain boundary conduction electrons may be subject to a strong spin-dependent scattering, which can be reduced if a low external magnetic field aligns the magnetizations of the two grains. Spin alignment in the disordered surface layers gives raise to high-filed magnetoresistance.

## 2.5. The known mechanism for manganites

### 2.5.1. Double exchange model

The behaviour of itinerant electron and ferromagnetism in the doped manganites is explained by Zener's double exchange mechanism. Manganese oxides, when doped, become ferromagnetic metals and exhibit remarkable magnetoresistive properties, which correlated ferromagnetism and metallic resistivity near $T_c$ [38]. According to that ferromagnetism arises from indirect coupling among the manganese ion spins via the carriers. Apart from this indirect coupling, there is super exchange between neighbouring $t_{2g}$ of antiferromagnetic character. The addition of divalent material in undoped LaMnO$_3$ changes the valence state of some $Mn^{3+}$ to $Mn^{4+}$. The $Mn^{3+}$ ions in LaMnO$_3$ have three electrons in the $t_{2g}$ state and one electron in the $e_g$ state due to the crystal field splitting. Because of the strong Hund coupling and on-site Coulomb repulsion between $e_g$ electrons, LaMnO$_3$ is an antiferromagnetic insulator. The replacement of trivalent $La^{3+}$ ions with any divalent cations (e.g., $Ca^{2+}$, $Sr^{2+}$, $Ba^{2+}$ etc.), some Mn ions change to the $Mn^{4+}$ state without $e_g$ electrons (as holes). The vacant $e_g$ state of $Mn^{4+}$ makes it possible for $e_g$ electrons in surrounding $Mn^{3+}$ ions to hop into the $e_g$ state of $Mn^{4+}$ as long as the localized $t_{2g}$ spins of neighboring $Mn^{3+}$ and $Mn^{4+}$ ions are parallel.

**Creation of a hole**
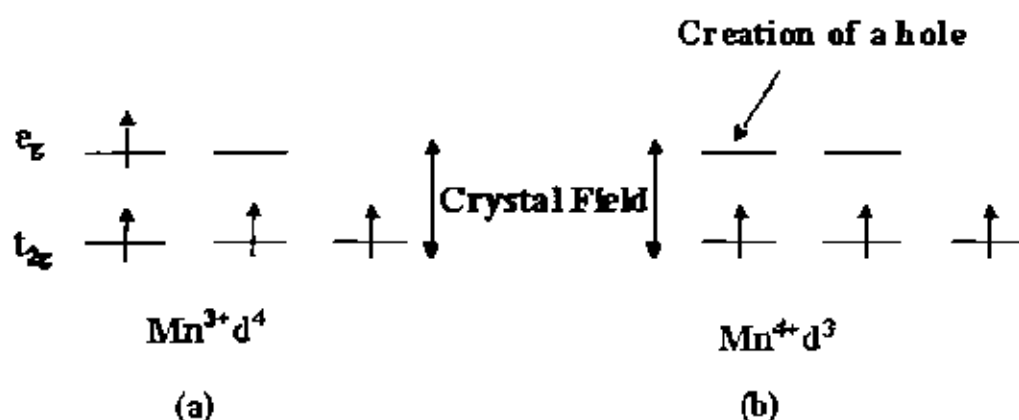


**Figure 2.13:** The splitting of the $t_{2g}$ and $e_g$ band in $La_{1-x}A_xMnO_3$.

In the perovskites structure the Mn ions are separated by $O^{2-}$ ions and conduction process occurs via oxygen as follows:

Before electron transfer:  $Mn^{3+}$  $O^{2-}$  $Mn^{4+}$

After electron transfer :  $Mn^{4+}$  $O^{2-}$  $Mn^{3+}$
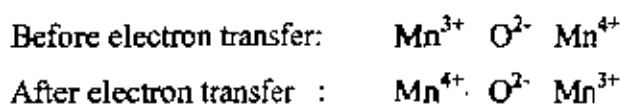
Jonker and Van Santeen [6-8], and Wollan and Koehler [32], concluded that the exchange coupling in general is: ferromagnetic between $Mn^{3+}$ and $Mn^{4+}$ ions, antiferromagnetic between $Mn^{4+}$ ions, either ferromagnetic or antiferromagnetic between $Mn^{3+}$ ions. The $T_c$ is related to the strength of the transfer integral between $Mn^{3+}$ and $Mn^{4+}$ ions. It can be expected that this coupling is strongly dependent on the angle subtended by the $Mn^{3+}$-O-$Mn^{4+}$ bond. It is found that $T_c$ is reduced by bending the $Mn^{3+}$-O-$Mn^{4+}$ bond.

### 2.5.2. Importance of double exchange model

Double exchange (DE) mechanism is very important for understanding the behaviour of manganite perovskites. This simple looking model has been deeply studied and, in certain regimes, qualitative agreement with experiment has been found. In particular, magnetic properties are better described than electric properties (there is not a M-I transition for DE). But some manganites, a hole doped $La_{1-x}Sr_xMnO_3$, are metallic for the whole range of temperatures (Fig.2.14). The fact is that lattice distortions compete with

the bandwidth and a large bandwidth (as is the case of $La_{1-x}Sr_xMnO_3$) implies a more efficient double exchange interaction. In fact, Varma [65] and, more recently, Lyanda-Geller et al. [66] have pointed out that Jahn-Teller phonons are not necessary to get the metal-insulator transition and double exchange plus disorder, which leads to localization as proposed.
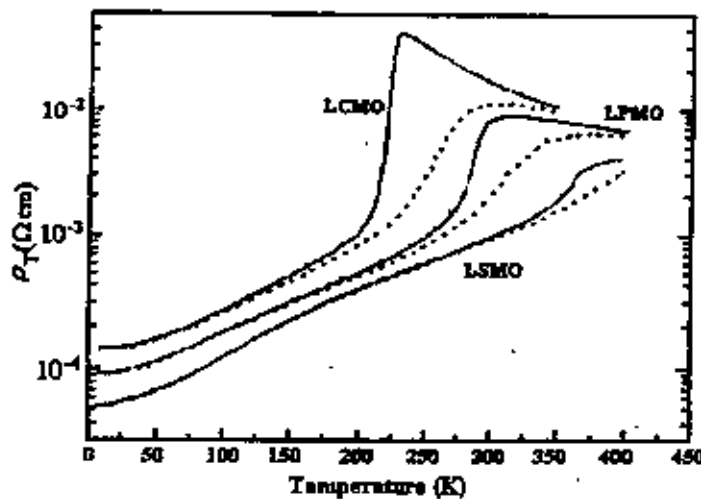


**Figure 2.14:** Temperature dependence of resistivity under zero magnetic field (solid lines) and other 7 $T$ (dotted lines) for $La_{0.7}Ca_{0.3}MnO_3$, $La_{0.67}(Ca,Pb)_{0.33}MnO_3$ and $La_{0.7}Sr_{0.23}MnO_3$.

### 2.5.3. Jahn-Teller distortion

Three electrons in the $3d$ orbital of the manganese ions form a triplet state at low energy that remain bound to the ion, and because they all point in the same direction they have overall magnetic moment of 3/2. In contrast, the electrons in the highest energy level are shared with the oxygen ions, forming an energy band and hence conductivity of the material is largely controlled by the width of the band. Perovskite cubic structure showed in Fig.2.15 are actually distorted because cations A and B can have very different sizes producing tilting and twisting of the oxygen octahedral [67-69]. This distortion can be estimated by the Goldschmidt tolerance factor, t. For a cubic lattice t=1 and decreases as the difference in size between A and B increases. It has been found that for oxides ands fluorides the perovskite structure types are stable in the range $1.0 \geq t \geq 0.77$.

Tilting of the octahedra can be measured with the distortion of the Mn-O-Mn bond angle $\Theta$ - $\Theta = 180^0$ for cubic symmetry. For particular composition, $\Theta$ can be the range from $150^0$ to $180^0$. This distortion affects the conduction band which appears as hybridization of the $p$-level of the oxygen and the $e_g$ levels of the Mn, which in turn depends on the geometric arrangement of the ions. The larger the overlap, the wider the band. Orbital overlapping decreases with the distortion and the relation between the bandwidth $W$ and $\Theta$ has been estimated as $W \infty \cos^2 \Theta$ [70].

Also the residual resistivity value $\rho_0$ increases by orders of magnitude when the bond angle decreases. Bandwidth is closely related to the magnitude of the critical temperature $T_c$ that could be increased by chemical pressure, namely by choosing the right cations A and B (or equivalently, by the application of external pressure). Two parameters are important here, the mean value of the cation sizes $\langle r_{A/B} \rangle$ and its variance $\sigma^2 = \langle r_{A/B}^2 \rangle - \langle r_{A/B} \rangle^2$ [71]. The main result is that a decrease of the cation disorder implies an increase of the critical temperature. In the ideal case $\sigma^2 = 0$ and a $T_c$ as large as 520 $K$ could be achieved. Another cause of disorder is the larger size of $Mn^{3+}$ (~0.72) with respect to $Mn^{4+}$ (~0.5). This leads to a breathing distortion mode as shown in Fig.2.15.
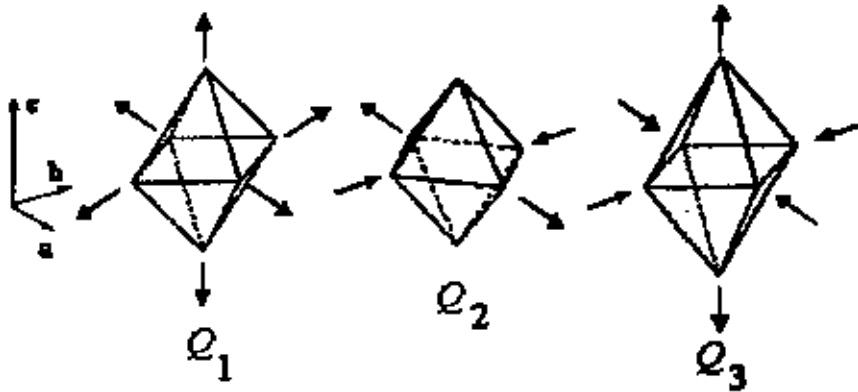


**Figure2.15:** Q2 and Q3 are the two Jahn-Teller modes of distortion of the oxygen octahedra associated to the splitting of the eg levels of Mn3+ [29]. These particular cases correspond to Q2>0 and Q3> 0. Q1 is the breathing distortion that occurs the different size of $Mn^{4+}$ and $Mn^{3+}$.

For instance, a $Q_3$ mode favours the occupancy of an orbital elongate on the z-direction $(d_{3z^2-r^2})$. The interaction between the Jahn-Teller distortion modes and orbitals is called cooperative Jahn-Teller. Lattice distortion of the octahedra can be static or dynamic. When the carriers have certain mobility, the distortion of $Mn^{3+}$ and $Mn^{4+}$ ions are random and changes with time. Therefore, electron-phonon coupling arises and, in fact, Millis et al. [62] and Roder et al. [72] claimed that it is necessary to take account of the lattice vibrations to explain the change in the curvature of the resistivity close to $T_c$. Morever due to large Hund's coupling, magnetic polarons can also be formed.

As a test of all this, it is well known that manganese perovskites present structural phase transitions for small values of x. The structure is rhombohedral at high temperature and orthorhombic with the lattice parameter ($\sqrt{2}a_0$, $\sqrt{2}a_0$, $\sqrt{2}a_0$) superstructure of the elementary cubic perovskite cell at low temperature. The critical temperature of this transition is ~700 $K$ for x = 0 and decreases to 0 for x = 0.2. Asamitsu et al. [73] showed that this transition could be externally controlled by application of a magnetic field implying of a large spin-lattice coupling.

## 2.5.4. Electron-phonon Coupling and Subsequent Theories

The double exchange and subsequent theories can only explain the transport properties of manganites qualitatively. However, it overestimates the Curie temperature of most manganites, can not describe the huge magnitude of the CMR effect, underestimates the resistivity values in the paramagnetic phase by several orders, and can't account for the existence of various antiferromagnetic phases, charge/orbital ordering, phase separation scenario and strong lattice effects seen experimentally due to its inherent limitation for several manganites. In 1995 Millis et al. [62] incorporated the idea that double exchange alone does not explain the resistivity of $La_{1-x}Sr_xMnO_3$. Their argument hinges mainly on an estimate of the Curie temperature in a pure double-exchange model which comes out to be an order of magnitude larger. Moreover, Millis et al. calculated the resistivity within the double-exchange model including spin fluctuations and found that resistivity decreases below $T_c$ and a positive magnetoresistance above $T_c$, both features in contradiction to the experimental results. Millis et al. argued that the electron-phonon coupling due to the dynamic Jahn-Teller distortion plays an important role, and that a strong interplay between electron-phonon coupling, including charge localization, and

Hund's coupling, generating a FM metallic phase, is responsible for the observed properties of manganites. The strong e-ph coupling in manganites is mainly caused by the Jahn-Teller effect of $Mn^{3+}$. The JT effect causes local distortion of the crystal structure in which some of the Mn-O bonds become shorter and other longer. This breaks the local cubic symmetry and splits the degeneracy of the $e_g$ levels on that site. By occupying the orbital with the lowest energy, the $e_g$ electron can become effectively self-trapped to form together with the surrounding deformed lattice a quasi-particle called lattice polaron or Jahn-Teller polaron. This transport of lattice and spin distortions is also called as magnetic-polaron. Calculations by Millis *et al.* predict the localization of charge carriers by temporal and spatial JT distortions around and above Tc. This would lead to the observed activated resistivity behaviour in the paramagnetic phase. Below Tc, the self-trapping of carriers ends leading to a relaxation of the lattice and an enhancement of the conductivity. In this theory both JT coupling and DE are needed to explain the properties in the various magnetic phases. This leads to the prediction of lower more correct $T_c$ values, and can explain the high resistivity and large CMR effect in manganites.

Roder *et al.* [74] incorporated Jahn-Teller (electron-phonon) coupling into the double exchange model and suggested that the $e_g$ charge carrier becomes self trapped as localized lattice distortions with a spin polarization around the position of charge carrier, having a coherence length of the order of five Mn sites. These quasi-self trapped small polaron can therefore be called magnetoelastic polaron, since they are associated with spin clusters and essentially form metallic islands in a paramagnetic lattice. Ample experimental evidence regarding the existence of magnetic polaron has been reported. It has been demonstrated by neutron diffraction that for both perovskite [75] and layered manganites [76], a volume reduction and relaxation of lattice is observed as the temperature decreases below $T_c$. This is due to change in the Mn-O bonds and indicates the existence of localized $e_g$ electrons above $T_c$ which becomes delocalized in the ferromagnetic phase.

## 2.5.5. Ordering Phenomenon

A fascinating phenomenon of charge ordering (CO) is found to occur in various transition metal oxides (TMO) wherein electron becomes localized due to ordering of cations of different charges (oxidation states) on specific lattice sites. Such ordering generally localizes the electrons in the material, rendering it insulating or semiconducting. This phenomenon of CO is well known in $Fe_3O_4$ which undergoes a disorder-order transition accompanied by a resistivity anomaly, popularly known as Verwey transition, at 120K [77,78]. CO has been found to occur in a few other TMO as well but the evidence of CO in doped rare earth manganites is overwhelming due to the discovery of Colossal Magnetoresistance and other interesting properties. The first evidence of CO in these rare earth doped manganites was observed by Wollan and Koehler [49] in their classic study through neutron diffraction and later examined by Jirak *et al* [79].

The general tendency of charge carrier localization and ordering in doped Mott insulators is particularly strong in doped manganites, due to the relatively enhanced carrier-lattice coupling. In addition, there exists orbital degree of freedom of the $e_g$ electrons in $Mn^{3+}$ ions. This orbital ordering can lower the electronic energy through the Jahn-Teller mechanism. Therefore, there exists orbital ordering (OO), in addition to charge ordering in mixed valent manganites. The first direct evidence of charge ordering in $La_{0.5}Ca_{0.5}MnO_3$ ($T_c \approx 220K$) was provided by electron diffraction studies reported by Chen and Cheong [80].

Radaelli *et al.* [81] reported a detailed synchrotron X-ray and neutron diffraction investigations of 50% Ca doped $LaMnO_3$. They observed weak satellites reflection in X-ray diffraction pattern which was consistent with that of Chen and Cheong. In $La_{1/3}Ca_{2/3}MnO_3$, there are twice as many $Mn^{4+}$ ($3d^3$) ions as the $Mn^{3+}(3d^4)$ ions, and the ordering of diagonal rows of $Mn^{4+}$ and $Mn^{3+}$ ions plus the orientational ordering of the $d_z^2$ orbital in $Mn^{3+}$ gives rise to the striped pattern.

Mori *et al.* [82] have reported a different pattern of charge localization in the charge-ordered phase of $La_{1-x}Ca_xMnO_3$ ($x \geq 0.5$) employing transmission electron microscopy at 95K. They observed extremely stable pairs of $Mn^{3+}O_6$ octahedra, with associated large lattice contraction (due to the Jahn-Teller effect), separated periodically by stripes of

non-distorted $Mn^{4+}O_6$ octahedra. These periodicities, which adopt integer values between 2 and 5 times the lattice parameter of the orthorhombic unit cell, corresponds to the commensurate carrier concentrations of $x=1/2$, $2/3$, $3/4$ and $4/5$; for other values of $x$, the pattern of charge ordering is a mixture of the two adjacent commensurate configuration. These paired Jahn-Teller stripes appear therefore to be the fundamental building blocks of the charge-ordered state in the manganites.

Recently, Loudon et al. [83] have observed charge ordering (CO) to ferromagnetic (FM) phase in $La_{0.5}Ca_{0.5}MnO_3$ employing Lorentz electron microscopy at 90K. They observed an inhomogeneous mixture of ferromagnetic and antiferromagnetic regions which extend for several micrometers, and can span several crystallographic grains. Loudon et al. have suggested that CO occurs not only in regions with no net magnetization, but can also occur in ferromagnetic regions this is consistent with the similar coexistence in $La_{0.25}Pr_{0.375}Ca_{0.375}MnO_3$ as observed by Mori et al. Very recently G. Van. Tendeloo et al. [84] have extensively reviewed the structure and microstructural aspects of colossal magnetoresistive materials with special reference to charge ordering.

### 2.5.6. Phase Separation (PS) Scenario

The physics of solids with strongly correlated electrons such as transition metal oxides (TMO) and related compounds appears to be dominated by states that are microscopically and intrinsically inhomogeneous in the most interesting range of temperatures and charge carrier densities. The most relevant examples are the cuprates at the hole densities in the underdoped region and the manganites in the regime of Colossal Magnetoresistance. In cuprates the competition occurs between antiferromagnetic insulating and superconducting or metallic phases. On the other hand in manganites the inhomogeneities arise from phase competition between ferromagnetic metallic and charge ordered insulating phases. These microscopic and intrinsic inhomogeneities lead to phase separation (PS) in manganites [83,84]. Indeed, the existence of phase separation was envisioned by Nagaev [85] in an antiferromagnetic semiconductor where the doping of electrons is expected to create ferromagnetic phase embedded in antiferromagnetic matrix. Nagaev remarked that if the two phases have opposite charge, the coulomb forces would break the macroscopic clusters into microscopic one, typically of nanometer scale size. Percolative transport has been considered to result from the coexistence of

ferromagnetic metallic and insulating phases. The tendency of PS is entirely reversible, and is generally the result of a competition between charge localization and de-localization, the two situations being associated with contrasting electronic and magnetic properties. These intrinsically inhomogeneous states are more pronounced and universally accepted for manganites. These phase-separated states give rise to novel electronic and magnetic properties with CMR in doped perovskite manganites.

The first evidence of phase separation in manganites was given in the pioneer neutron diffraction study of $La_{1-x}Ca_xMnO_3$, by Wollan and Koehler [32] in 1955. They reported the coexistence of ferromagnetic and A-type antiferromagnetic reflections in non-stiochiometric $LaMnO_3$ (14, 18 and 20% $Mn^{4+}$) and in $La_{0.89}Ca_{0.11}MnO_3$. The most important results that have convincingly shown the presence of coexisting clusters of metallic and insulating phases in the CMR regime of manganites was obtained by Uehera *et al.* [86] in their study of $La_{5/8}PrYCa_{3/8}MnO_3$ using transport, magnetic and electron microscopy techniques. They observed an enormous low temperature resistivity in spite of the fact that $\partial \rho / \partial T > 0$ suggests metallic behavior. By itself this shows that a homogenous picture of manganites will likely fail, since only a percolative state can produce such large but metallic resistivity. The magnetoresistance is large and increases rapidly as $T_c$ is reduced.

Another remarkable evidence of mixed phase tendencies in $La_{0.7}Ca_{0.3}MnO_3$ single crystals and thin films has been given by Fath *et al.* [87] employing scanning tunneling spectroscopy (STS). Below Tc, phase separation was observed where inhomogenous clusters of metallic and insulating phases coexist. Very recently D. D. Sarma *et al.* [88] observed the formation of distinct electronic domains by direct spatially resolved spectroscopy.

In short we can say that the instability towards phase separation and the formation of inhomogeneous states or competing phases, e.g. CO/AF and FM, is an intrinsic property of doped perovskite manganites. The existence of these performed clusters (inhomogeneous state or competing phase of CO/AF and FM) and their easy alignment with modest magnetic fields leads to Colossal Magnetoresistance.

### 2.5.7. Phase diagram and resistivity:

Phase diagram of doped perovskite manganites are exceptionally rich with different magnetic as well as structural phases. The phase diagrams that have been established so far for different compounds e.g. $La_{1-x}Ca_xMnO_3$, $La_{1-x}Ba_xMnO_3$, $La_{1-x}Sr_xMnO_3$ etc. are constructed from detailed measurements of macroscopic physical quantities such as resistivity, susceptibility and magnetization on single crystal and bulk ceramic samples. Even though the phase diagram of each composition is different due to the variation in sizes of different atoms involved but they have some common features. $La_{1-x}Ca_xMnO_3$ is a good candidate material for basic understanding and hence its phase diagram has been described in detail. CMR manganites are oxides of the type $RE_{1-x}\ AE_xMnO_3$, where R denotes a rare earth and A is a divalent, often alkaline earth element.

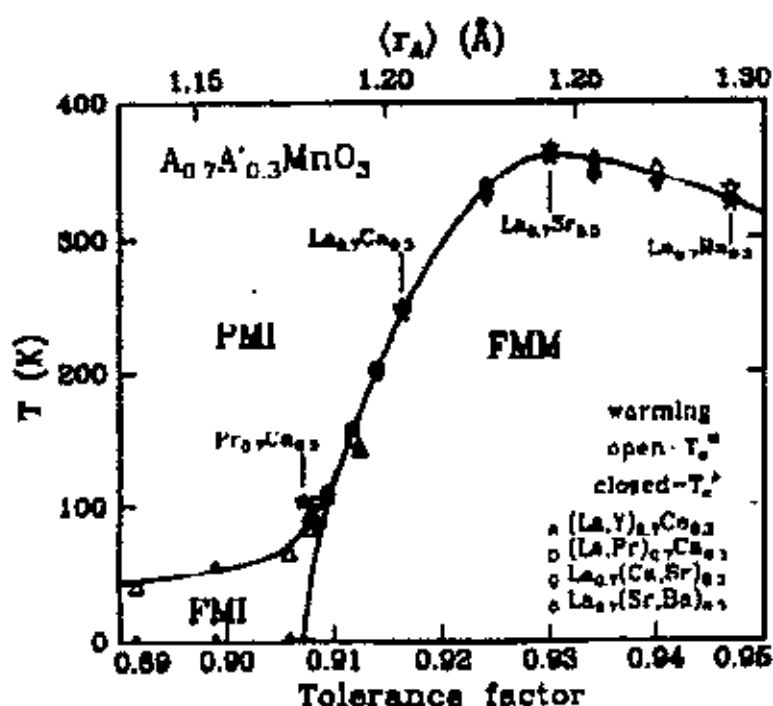Much interest has been devoted to the CMR manganites, since these displays a diversified phase diagram.



**Figure 2.16.** Phase diagram of temperature versus tolerance factor for $A_{0.7}A'_{0.03}\ MnO_3$, where A is a trivalent ion and A' a divalent ion. Open symbols denote $T_C$ determined by magnetization measurements and closed symbols denote $T_C$ determined by resistivity measurements. All data were taken while warming.

42

In figure 2.16 at low temperature the resistivity is metallic , rising sharply while going through the ferromagnetic transition and showing semiconducting behavior in the paramagnetic phase in the case of Ca doping , whereas the resistivity in the case of Sr doping remains metallic above the Curie temperature .accordingly , the ferromagnetic transition in this case compound is accompanied by a metal- insulator transition as evidence by the resistivity rise and the negative temperature coefficient of the resistivity in most compounds above $T_c$ .

## 2.6.    Magnetic-based device

Recent progress in oxide perovskites thin film technology has led to the discovery of a large negative magnetoresistance at room temperature which open up new avenues for applications in diverse area of technology such as magnetic random access memories and reads heads for hard disc drives. Based on the properties of manganites, a number of device approaches are being explored, some of which are discussed here briefly.

(i)     Magnetic field sensors (a) using the CMR effect in a film, (b) using a spin valve structure and (c) as a microwave CMR sensors. The industrial requirements for a magnetic sensor are operation at room temperature and up to 400 $K$, at least a 20% MR at a field   10 $mT$ applied field, temperature dependent CMR values over $350 \pm 50$ $K$ and acceptable noise values. The current thinking is that oxide-based CMR sensors will have maximum impact only on memory systems approaching densities of 100 GB $cm^{-2}$.

(ii)    Electric field effect devices (a) using a $SrTiO_3$ gate and (b) using a ferroelectric gate. Field effect transistors (FET) based on CMR channels show some interesting characteristics depending on the dielectric layer on top as to whether it is a paraelectric layer such as STO, or a ferroelectric layer such as PZT. The advantage of these devices unlike conventional NVRAM would be that the reading of the state of the memory would be direct since the resistance is considerably different.

43

(iii)    Low temperature hybrid *HTS-CMR* devices: As the properties of *CMR* materials are quite spectacular at reduced temperatures, i.e., below 100*K*, there may some advantages to integrating them with *HTS* devices.

(iv)    Room Temperature Bolometric Infrared (*IR*) Sensors: Due to the advance in thermoelectric cooling, materials with high thermal nonlinearities in the temperature range of 250 to 300 *K* are potential candidates for bolometric sensors.



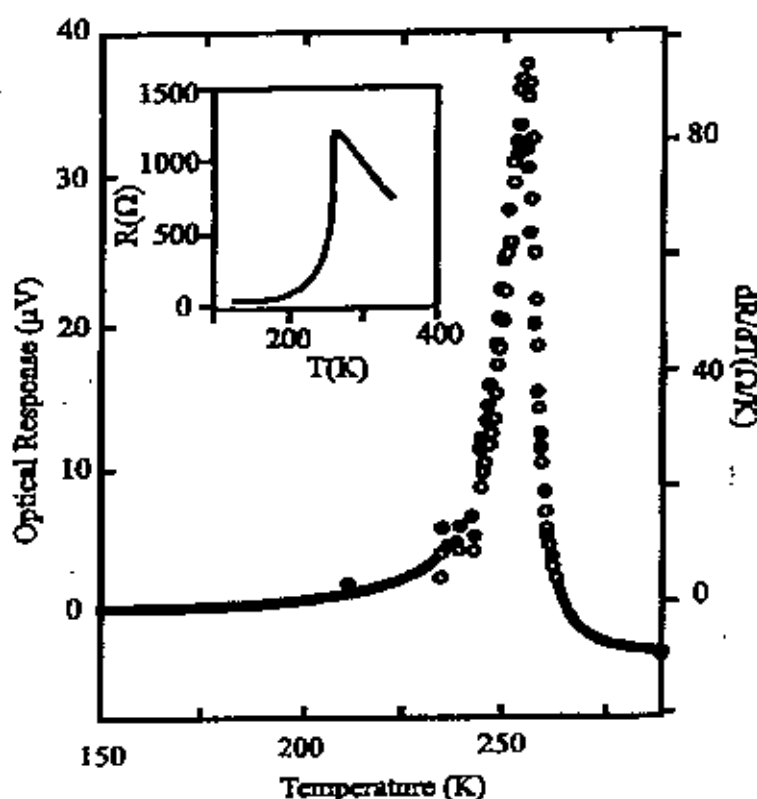**Figure 2.17:** Optical response of a film of LCMO (closed circles) in comparison with   the TCR (open circles). The curve is shown in the inset.

The commercial bolometers based on $VO_x$ used now a days use temperature coefficient of resistance of resistance (TCR) values around 2.5% to 4%. In comparison TCR values ranging from 8% to 18% are possible in the LCMO manganites over the same temperature range (figure. 2.17).

# References:

[1] Rao C N R and Raveau B, "Transition Metal Oxides: Structure, Properties and Synthesis of Ceramic Oxides" John Willey and Sons, Inc. (1998).

[2] Srivastava O N , Siwach P K, Singh H K, "Low Field Magnetotransport in Manganites" Ph. D. thesis, Physics Department, Banaras Hindu University, India (2003).

[3] Prinz G A, "Magnetoelectronics", Science **282**, 1660 (1998).

[4] Wolf S A, Awschalom D D, Buhrman R A, Daughton J M, von Molnar S, Roukes M L, Chtchelkanova AY, and Treger D M, "Spintronics: A Spin-Based Electronics Vision for the Future", Science **294**, 1488 (2001).

[5] Ziese M and Thornton M J, "Spin Electronics", Springer Heidelberg (2001).

[6] Jonker G H, and van Santeen J H, "Ferromagnetic compounds of manganese with perovskite structure", Physica 16, 337 (1950).

[7] van Santeen J H, and Jonker G H, "Electrical conductivity of ferromagnetic compounds of manganese with perovskite structure", Physica **16**, 599 (1950).

[8] Jonker G H, and van Santeen J H, "Magnetic compounds with perovskite structure iii. Ferromagnetic compounds of cobalt ", Physica **19**, 120 (1953).

[9] Searle C W, and Wang S T, "Studies of the ionic fragment (La, Pb) $MnO_3$. v. Electric transport and ferromagnetic properties", Can. J. Phys. 48, 2023 (1970).

[10] Wang S T, and Searle C W, "Studies of the ionic fragment (La,Pb)$MnO_3$. vi. Antiresonance and the ferromagnetic resonance line shape properties", Can.J. Phys. **49**, 387 (1970).

[11] Chahara K, Ohno T, Kasai M, and Kozono Y, "Magnetoresistance in magnetic manganese oxide with intrinsic antiferromagnetic spin structure", Appl. Phys. Lett. **63**, (1993).

[12] von Helmholtz R, Wocker J, Holzapfel B, Schultz M. and Samwer K, "Giant negative magnetoresistance in perovskite like $La_{2/3}Ba_{1/3}MnO_3$ferromagnetic films", Phys Rev Lett 71, 2331(1993).

[13] Jin S, Tiefel T H, McCormack M, Fastnacht R A, Ramesh R, and Chen J H, "Thousand-fold change in resistivity in magnetoresistive La-Ca-Mn-O films", Science **264**, 413 (1994).

[14] Pippard A B, "Magnetoresistance", Cambridge University Press Cambridge UK (1984).

[15] Watts S M, Wirth S, von Molnar S, Barry F, and Coey J M D, "Evidence for two-band magnetotransport in half-metallic chromium oxide", Phys Rev B 61, 149621 (2000).

[16] Ashcroft N, and Mermin B, "Solid State Physics" Holt Rinehart and Winston New York (1976).

[17] Baibich M N, Broto J M, Fert A, Nguyen Van Dau F, Petroff F, Etienne P, Creuzet G, Friederich A, and Chazeles J, "Giant magnetoresistance of (001) Fe/(001) Cr magnetic superlattices," Phys. Rev. Lett. 61, 2472 (1988).

[18] Binasch G, Grunberg P, Saurenbach F, and Zinn W, "Enhanced magnetoresistance in layered magnetic structures with antiferromagnetic interlayer exchange ", Phys Rev B 39, 4828(1989).

[19] Parkin S S P, Li Z G, and Smith D J, "Giant magnetoresistance in antiferromagnetic Co/Cu multilayers," Appl. Phys. Lett. 58, 2710 (1991).

[20] Parkin S S P, More N, and Roche K P, "Oscillations in exchange coupling and magnetoresistance in metallic superlattice structures: Co/Ru, Co/Cr, and Fe/Cr" Phys Rev Lett 64, 2304 (1990).

[21] Parkin S S P, Bhadra R, and Roche K P, "Oscillatory magnetic exchange coupling through thin copper layers", Phys Rev Lett 66, 2152( 1991).

[22] Berkowitz A E, Mitchell J R, Carey M J, Young A P, Zhang S, Spada F E, Parker F T, Hutten A, and Thomas G , Phys Rev Lett 68 3745(1992).

[23] Xiao J Q, Jiang J S, and Chien CL, "Giant magnetoresistance in nonmultilayer magnetic systems", Phys Rev Lett 68, 3749 (1992).

[24] Hylton T L, Coffey K R, Parker M A, and Howard J K, Science 261, 1021 (1993).

[25] Gittlemann J I, Goldstein Y, and Bozowski S, "Magnetic Properties of Granular Nickel Films", Phys Rev B 5, 3609 (1972).

[26] Helman J S, and Abeles B, Phys Rev Lett 37, (21) 1429 (1976).

[27] Parkin S S P, and York B R, "Technical Article - Spin-Polarized Current in Spin Valves and Magnetic Tunnel Junctions", Appl Phys Lett 62, 1842 (1993).

[28] Grunberg P, Schreiber P, Pang Y, Brodsky M B, and Sower H, "Layered Magnetic Structures: Evidence for Antiferromagnetic Coupling of Fe Layers across Cr Interlayers", Phys Rev Lett 57, 2442(1986).

[29] Parkin S S P, Annu Rev Mater Sci **25**, 357(1995).

[30] Volgar J, "Further experimental investigations on some ferromagnetic oxidic compounds of manganese with perovskite structure", Physica **20**, 49 (1950).

[31] Jonker G H, "Semiconducting properties of mixed crystals with perovskite structure", Physica **20**, 1118 (1954).

[32] Wollan E O, and Koehler W C, " Neutron diffraction study of the magnetic properties of the series of perovskite-type compounds [ (1-x) La, x Ca] $MnO_3$", Phys. Rev. **100**, 545 (1955).

[33] Vratislva S, and Zajicek J, Phys Stat Sol (a) **52 K** 39 (1979).

[34] Pollert E, Krupicka S, and Kuzmicova E, "Structural study of $Pr_{1-x}Ca_xMnO_3$ and $Y_{1-x}Ca_xMnO_3$ perovskites", J Phys Chem Solids **43**, 1137 (1982).

[35] Kusters R M, Singleton J, Keen D A, McGreevy R, and Hayes W, "Magnetoresistance measurements of the magnetic semiconductor $Nd_{0.5}Pb_{0.5}MnO_3$," Physica B **155**, 362 (1989).

[36] Ju S, Sun H, and Li Z "Study of magnetotransport in polycrystalline perovskite manganites", Journal of Physics Condensed Matter, **14**, L631 (2002).

[37] Goodenough J B, "Magnetism and the Chemical bond ", (Huntington: Krieger) (1970).

[38] Zener C, "Interaction between d shells in the transition metals", Phys. Rev. **81**, 440 (1951).

[39] Zener C, "Interaction between d shells in the transition metals. ii. Ferromagnetic compounds of manganese with perovskite structure", Phys. Rev. **82**, 403 (1951).

[40] van Aken B B, "Structural response to electronic transitions in hexagonal and ortho-manganites", Ph D Thesis, Dutch foundation for Fundamental Research on Matter (MOF), University of Groningen, Netherlands, (2001).

[41] Naray-Sszabo S V, Naturwissenschaften **31**, 466 (1943)

[42] Yakel H L, Acta Crystallogr. **8**, 394 (1955)

[43] Rodriguez-Martinez L M, and Attfield J P, "Disorder-induced orbital ordering in $La_{0.7}M_{0.3}MnO_3$", Phys. Rev. B **63**, 024424 (2001).

[44] van Aken B B, "Structural response to electronic transitions in hexagonal and ortho-manganites", Ph D Thesis, Dutch foundation for Fundamental Research on Matter (MOF), University of Groningen, Netherlands, (2001).

[45]Elemans J-B A A, van Laar B, van der Veen K R, and Loopstra B O, "The crystallographic and magnetic structure of $La_{1-x}Ba_xMn_{1-x}Me_xO_3$", J. Solid State Chem. 238 (1971).

[46] Huang Q, Santoro A, Lynn J W, Rrwin R W, Borchers J A, Peng J L, and Greene R L, "Structure and magnetic order in undoped lanthanum manganite", Phys. Rev. B 55, 14987 (1997).

[47] Goodenough J B, "Magnetism and the Chemical bond ", (Huntington: Krieger) (1970).

[48] Pickett W E, and Singh D J, "Electronic structure and half-metallic transport in the $La_{1-x}Ca_xMnO_3$ system", Phys. Rev. B 53, 1146 (1996).

[49] Alvysdas Lisauskas, "Low frequency noise in thin film colossal magnetoresistance", Ph D Thesis, Department of Condensed Matter Physics at the Royal Institute of Technology, Sweeden, (2000).

[50] Pickett W E and Singh D J, "Electronic structure and half-metallic transport in the $La_{1-x}Ca_xMnO_3$ system", Phys. Rev. B 53, 1146 (1996).

[51] Satpathy S, Popovic Z S, and Vukajlovic F R, "Origin of charge orbital order in the half-doped manganites", Phys. Rev. Lett. 76, 960 (1996).

[52] Park J H, Chen C T, Cheong S W, Bao W, Meigs G, Chakarian V, and Idzerda Y U, "Electronic aspects of the ferromagnetic transition inmanganese perovskites", Phys. Rev. Lett. 76, 4215 (1996).

[53] Dessau D S, and Shen Z X, "Direct electronic structure measurements of the Colossal magnetoresistive Oxides", A Chapter in "Colossal Magnetoresistive Oxides", Edited by Y.Tokura, Monographs in condensed matter Science, Gordon and Breach, London 1998.

[54] Gupta A, Gong G Q, Xiao G,.Duncombe P R, Lecoeur P, Trouilloud P, Wang Y Y, Dravid V P, and Sun JZ, "Grain boundary effects on the magnetoresistance properties of perovskite manganite films", Phys. rev. B, 54 (22), R15629 (1996).

[55] Li X W, Gupta A, Xiao G, and Gong G Q, "Low-field magnetoresistive properties of polycrystalline and epitexial perovskite manganite films", Appl. Phys. Lett., 71 (8), 1124 (1997).

[56] Ju S, Sun H, and Li Z, "Study of magnetotransport in polycrystalline perovskite manganites", Journal of Physics Condensed Matter, 14, L631 (2002).

[57] Hwang H Y, Cheong S W, Ong N P, and Batlogg B, "Spin-Polarized Intergrain Tunneling in $La_{2/3}Sr_{1/3}MnO_3$,", Phys. Rev. Lett. 77, 2041 (1996).

[58] Evetts J E, Blamire M G, Mathur N D, Isaac S P, Teo B, Cohen L F, and Macmanus-Driscol J L, "Defect-induced spin disorder and magnetoresistance in single-crystal and polycrystal rare-earth manganite thin film", Philosophical Transactions of the Royal Society, London A, 356, 1593 (1998).

[59] Hundley M F, Hawley M, Heffner R H, Jia Q X, Neumeier J J, and Teamer J, "Transport-magnetism correlations in the ferromagnetic oxide $La_{0.7}Ca_{0.3}MnO_3$" Appl. Phys. Lett. 67 (6), 860 (1995).

[60] Coey J M D, Viret M, and Von Molnar S, "Mixed-valence manganites", Advances in physics, 48(2) 167,(1999).

[61] Von Helmolt R, Wecker J, Haupt L, and Barner K, "Intrinsic giant magnetoresistance of mixed valence La-A-Mn oxide (A=Ca,Sr,Ba)", J. Appl. Phys. 76 (10) 6925 (1994).

[62] Millis A J, Mueller R, and Shraiman B I, " Fermi-liquid to polaron crossver.ii: Double exchange and the physics of colossal magnetoresistance", Phys. Rev. B 54 5405 (1996).

[63] Okimoto Y, Ishikawa T, Katsufuji T, Urashibara A, Arima T, and Tokura Y, "Anomalous variation of optical specta with spin polarization in double-exchange ferromagnet: $La_{1-x}Sr_xMnO_3$", Phys. Rev. Lett. 75(1), 109,(1995).

[64] Tumanski S, " Thin film magnetoresistive sensors" Bristol: Institute of Physics Publishing (2001).

[65] Varma C M, "Electronic and magnetic states in the giant magneto-resistive compounds", Phys. Rev. B 54, 7328 (1996).

[66] Lyanda-Geller Y, Chun S H, Salamon M B, Golbart P M, Han P D, Tomioka Y, Asamitsu A, and Tokura Y, "Charge transport in manganites: hopping conduction, the anomalous hall effect and the universal scaling", condo-mat/0012462 (2000).

[67] Tomioka, Asamitsu A, and Tokura Y, "Charge transport in manganites: hopping conduction, the anomalous hall effect and the universal scaling", condo-mat/0012462 (2000).

[68] Alvysdas Lisauskas, "Low frequency noise in thin film colossal magnetoresistance", Ph D Thesis, Department of Condensed Matter Physics at the Royal Institute of Technology, Sweeden, (2000).

[69] Fontcuberta J, Martinez B, Seffer A, Pinol S, Garcia-Munoz J L, and Obradors X "Colossal magnetoresistance of ferromagnetic manganites: structural tuning and mechanisms", Phys. Rev. Lett. 76, 1122 (1996).

[70] Rodriguez-Martinez L M, and Attfield J P, "Disorder-induced orbital ordering in $La_{0.7}M_{0.3}MnO_3$", Phys. Rev. B 63, 024424 (2001).

[71] Radaelli P G, Iannon G, Marezeo M, Hwang H Y, Cheong S W, Jorgensen J D, and Argyriou D N, "Structural effects on the magnetic and transport properties of perovskite $A_{1-x}A_x'MnO_3(x=0.25, 0.30)$", Phys. Rev B 56, 8265 (1997).

[72] García-Muñoz J L, Fontcuberta J, Susaidi M, and Obradors X, "Band-width narrowing in bulk $La_{2/3}A_{1/3}MnO_3$ magnetoresistive oxides", J. Phys.: Condens. Matt. 8, L787 (1996).

[73] Asamitsu A, Moritomo Y, Tomioka Y, Arima T, and Tokura Y, "A structural phase transition induced by an external magnetic field", Nature 373, 407 (1995).

[74] Röder H, Zang J, and Bishop A R, "Lattice effects in the colossal magneto- resistance manganites", Phys. Rev. Lett. 76, 1356 (1996).

[75] Okimoto Y, Ishikawa T, Katsufuji T, Urashibara A, Arima T, and Tokura Y, "Anomalous variation of optical specta with spin polarization in double-exchange ferromagnet: La1-xSrxMnO3" Phys. Rev. Lett. 75(1), 109,(1995)

[76] Kaplan S G, Quijada U M, Drew H D, Tanner D W, Xiong G C, Ramesh R, Kwon C, and Venkatesan T, "Optical Evidence for the Dynamic Jahn-Teller Effect in $Nd_{0.7}Sr_{0.3}MnO_3$", Phys Rev Lett 77, 2081 (1996).

[77] Achutharaman V S, Kraus P A, Vasko V A, Nordman C A, and Goldman A M, Appl Phys Lett 67, 1019 (1995).

[78] Mitchell J F, Argyriou D N, and Jorgensen J D, "Colossal Magnetoresistance Oxide" Y Tokura (ed) Gordon and Breach London (and reference therein) 2000.

[79] Jirak Z., Vratislva S, and Zajicek J, Phys Stat Sol (a) 52 K 39 (1979).

[80] Chen C H, Cheong S W, and Cooper A S , "Charge modulations in $La_{2-x}Sr_xNiO_{4+y}$: Ordering of polarons", Phys Rev Lett 71 2461(1993).

[81] Radaelli P G, Iannon G, Marezeo M; Hwang H Y, Cheong S W, Jorgensen J D, and Argyriou D N, "Structural effects on the magnetic and transport properties of perovskite $A_{1-x}A_x'MnO_3(x=0.25, 0.30)$", Phys. Rev B 56, 8265 (1997).

[82] Mori S, Chen C H, and Cheong S W, "Pairing of charge-ordered stripes in (La,Ca)MnO3" Nature 392, 473 (1998).

[83] Loudon J C, Mathur N D, and Midgley P A, "Charge ordered ferromagnetic phase in $La_{0.5}Ca_{0.5}MnO_3$", Nature **420**, 797(2002).

[84] Van Tendeloo G, Lebedev O I, Hervieu M, and Raveau B, Rep Prog Phys 67 1315(2004).

[85] Nagaev E L "Physics of Magnetic Semiconductors" Mir Publisher Moscow(1986).

[86]. Uehara M, Mori S, Chen C H, and Cheong S W, "Percolative phase separation underlies colossal magnetoresistance in mixed-valent manganites" Nature **399**, 560(1999).

[87] Fath F, Freisem S, Menovsky A A, Tomioka Y, Aarts J, and Mydosh J A, Science 285 1540 (1999).

[88] Sarma D D, Topwal D, Manju U, Krishnakumar S R, Bertolo M, La Rosa S, Cautero G, Koo T Y, Sharma P A, Cheong S W, and Fujimori, "Magnetoresistance in order and disordered double perovskite oxide $Sr_2FeMoO_6$", A cond-matt/0409343 (2000).

# Chapter 3

## Sample Preparation and Experimental Setup

In this chapter, experimental methods of sample preparation and characterization techniques are discussed. A brief description of the apparatus, used in the measurements also given. Basic techniques of sample preparation and experimental technique are disclosed in this chapter.

### 3.1 Preparation of the samples:

Samples can be prepared mainly using any of the following method:

1. Solid state reaction method.

2. Solution method.

3. Melt- quenched or glass ceramic method.

4. Thin film method.

### 3.1.1 Solid State reaction method

In solid state reaction method appropriate amounts of two or more chemicals are carefully grind together and mixed thoroughly in a mortar and pestle or ball mills. Grinded powders are then calcined in air or oxygen at a temperature above 750 °C for several hours. This process is continued for several times until the mixture is converted into the correct crystalline phase. This calcined material are then grinded to fine powders and pelletized in a hydraulic press followed by sintering at different temperature below the melting point of the materials in air or any controlled atmosphere.

### 3.1.2. Solution method

In this method appropriate amount of solid chemicals are at first dissolved in nitric acid. This solution is then dried and then followed by calcination and sintering treatments. Some times water soluble materials such as nitrates are used for synthesizing superconducting ceramic materials. The nitrates are dissolved in water and then dried and calcined in a way similar to the solid state reaction method.

### 3.1.3 Melt-quenched or glass ceramic method:

In this method appropriate amounts of mixed powder are taken in oxide or carbonate crucible and calcined for one to two hours below the melting point of the material. After

calcination the powders are melted at few hundred-degree Celsius above the melting temperature and held there for a couple of hours. The melts are then poured into a cold iron or brass plate and pressed quickly by another plate to 1 to 2 mm thick sheets. The glasses thus obtained are then annealed at suitable temperature for different periods of time in air or in any controlled atmosphere.

### 3.1.4 Thin film method

Thin films of superconducting materials have been very successfully fabricated using the procedure like, Evaporation, Sputtering, Ion Beam sputtering, Laser Evaporation etc. Evaporation is conceptually the simplest of all the deposition techniques. In practice, however, some of the most sophisticated apparatus are used to evaporate epitaxial films of materials under very controlled conditions and these systems are more accurately called molecular electron beam epitaxy system (MBE\EBE). The technique involved utilizes a vacuum system to remove most of the contaminating gases from the deposition chamber. Typical pressures that are obtained in simple evaporations are in the $10^{-7}$ torr range until the MEB\EBE system requires pressures of less than $10^{-10}$ torr. The elements or compounds to be evaporated are heated in crucibles by either resistive heating elements or by electron beam heating. Typical evaporations have more than one evaporation source, and it is possible to obtain systems with as many as six independent sources. The high temperature produced in these sources cause the vapor pressure of the evaporation rise to a level at which a significant amount of these materials can be collected on a substrate that is located on a direct optical path from the evaporate. The substrate can typically be at a variety of temperatures, ranging from 77 K to approximately 1300 K depending on the required microstructure of the final film. The substrate materials are sapphires $Al_2O_3$, MgO, silicon etc.

### 3.2.1 Procedure for the preparation of the present samples

For the present investigation, Polycrystalline samples of $La_{n-nx}Ca_{1+nx}Mn_{n-y}Cr_yO_{3n+1}$ ($x = 0.3$; $y = 0.075, 0.15, 0.3$; $n = 2, 3$) were synthesized using the conventional solid state reaction method. Raw materials $La_2O_3$ (99.99%), $CaCO_3$ (99.99%), $Cr_2O_3$ (99.99%) and $MnCO_3$ (99.99%) were mixed in stoichiometric amount. The chemicals were weighed out separately using an electronic Digital analytical balance (measuring range 0.0001-210g), weight being shown by LED display and then well mixed and grind in a ceramic

mortar using a pestle for 6 to 8 hours in dry and acetone media. The grayish powder thus obtained in the mortar was scraped from its wall and was poured into alumina crucible. Crucible was previously washed with nitric acid, distilled water, then with acetone. The crucibles with the powder then placed in the furnace for calcinations purpose.

### 3.2.3 Calcination schedule

The grinded powders were calcined in air or in oxygen at a temperature 1373 $K$ ($1100^0$ $C$) to remove the unwanted oxides present in the chemicals. The temperature controller was set at 1100°C for 5 hours. After 8 hours it was cooled to room temperature (Furnace cooling). When room temperature was attained, the chunk was regrinded and reheated until the mixture is converted into the correct crystalline phase. The above procedure was repeated further for two times.

### 3.2.4 Pellets:

Calcined powders are shining black powders. These calcined powders were grinded again to fine powders and pressed into pellets of 12 mm diameter and 1-2 mm thick under a pressure of 6000 PSI for about 1 to 2 minutes using hydraulic pressure machine.

### 3.2.5 Sintering and oxidation:

The pellet formed inside the mould had a shiny black surface. It was again placed in a boat and inserted into the furnace for sintering and oxidation. Sintering was done at 1573K (1300°C) in air for 1 hour. The temperature ramp was 10°C/minute for both cooling and heating. The pellets were then ready for measurements.

### 3.3 Methodology

The DC electrical resistivity for various polycrystalline samples were measured from room temperature down to liquid nitrogen temperature using standard four-probe method. The temperature dependence of normalized resistivity, $\rho(T)/\rho(RT)$ at zero applied magnetic field for various polycrystalline samples and the corresponding behaviour in presence of 0.7 $T$ applied magnetic field have been taken. Magnetoresistance measurements were carried out in a magnetic field of around 0.7 Tesla in the temperature range 78 $K$ to 300 $K$.

### 3.4 Apparatus used for the present investigation

### 3.4.1 Description of Liquid Nitrogen Cryostat

A liquid nitrogen cryostat is designed for the purpose of low temperature magneto-transport measurements. It is made up of nonmagnetic concentric stainless steel tubes. It consists of two parts (upper part and lower part) and each part consists of three concentric tubes of three different dimensions. The outer diameter of the upper part of the cryostat is 7.6 cm and inner diameter is 3.2 cm. The outer diameter for lower part is 3.8 cm and inner diameter is 3.2 cm. It has three chambers as shown in Figure 3.1. Outer chamber is called vacuum chamber the middle one is cryogen (liquid nitrogen) chamber and the innermost chamber is sample space. Thickness of the wall of each chamber is about 0.2 cm. In the top of the second chamber there are two small pipes connected over the stainless steel plate of upper part of the cryostal, one for inlet of liquid nitrogen and the other for outlet of nitrogen gas. The lower part (20 cm long and 3.8 cm diameter) of the cryostat is shorter and narrower compared to the upper part (85 cm long and 7.6 cm diameter). It is made in such a way that the lower part of the cryostat can easily move between the pole pieces of the home made electromagnet. A stainless steel plate connects the lower part and upper part. The top of the upper part is sealed by another stainless steel plate. In the innermost chamber (sample space) there is a sample rod which is made up of stainless steel tube and a flat copper bar. The diameter of the sample rod is chosen in such a manner that it can easily move through the sample space. The top of the sample rod and innermost tubes are air tight connected with a union socket. A thermocouple is used for the measurement of temperature of the sample. It was observed that if the cryostat is filled with liquid nitrogen than it takes about 150 minutes to warm up to room temperature.
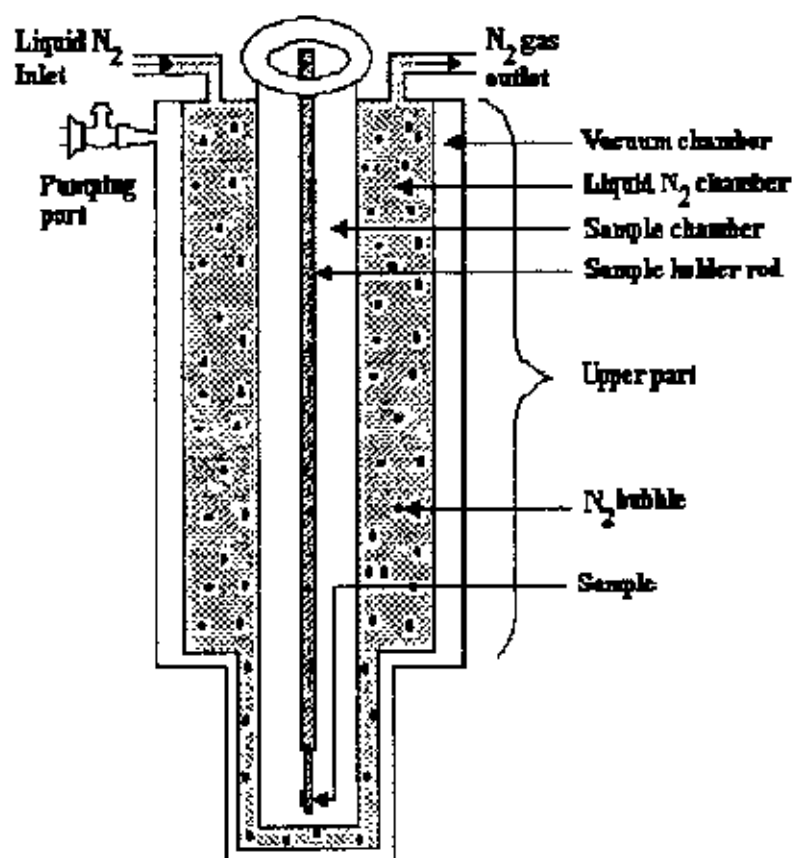
**Figure 3.1:** Schematic diagram of the liquid nitrogen cryostat.

### 3.4.2 Description of Electromagnet

To study magneto-transport properties of manganese perovskites the electromagnet used is shown in Figure 3.2. Materials play an important role for designing an electromagnet. Normally soft iron with a very low coercive field and low hysteresis is used for the magnet pole pieces. Commercial mild steel bar is used for the body of the electromagnet and soft iron cylindrical rod for pole pieces, which are available in the local market (Dhaka, Bangladesh).
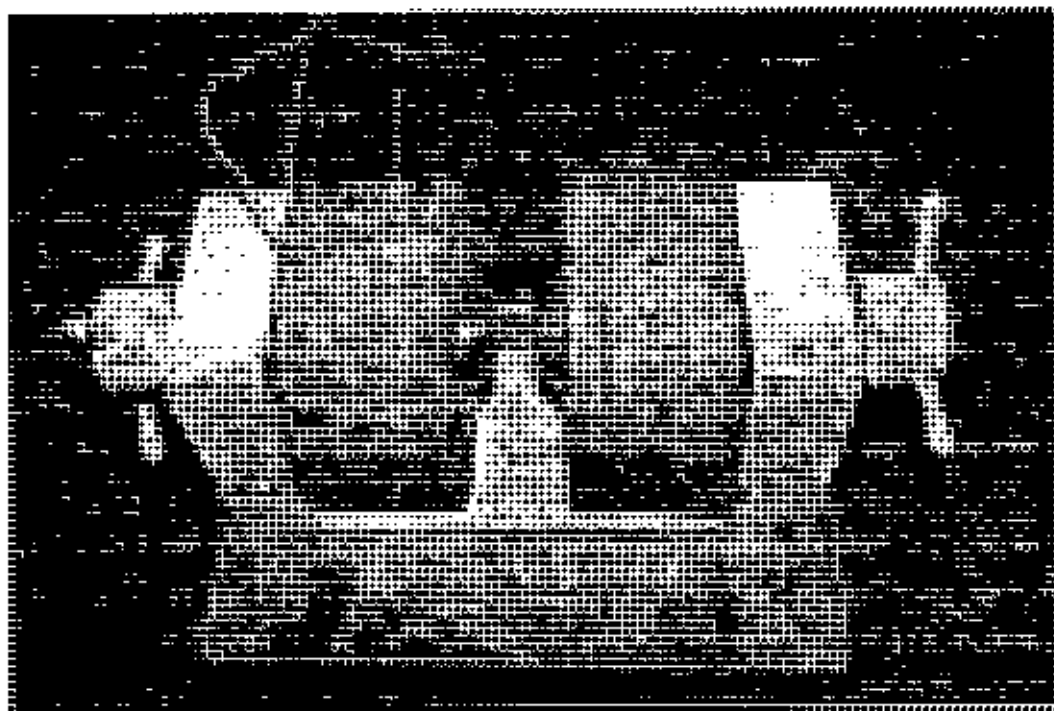
**Figure 3.2:** Schematic diagram of the Electromagnet.

The major parts of the electromagnets are base, pole piece holder, pole pieces and coils. Base of the electromagnet is made up of a parallelepiped shaped mild steel bar of dimension 36 cm × 19 cm × 8 cm. Pole piece holder of the electromagnet is also made from commercial mild steel bar. Two pole piece holders are attached to both side of the base with L type bolt. Each pole piece holder is a parallelepiped of dimension 32 cm×19 cm×8 cm. Pole pieces (cylindrical soft iron of final diameter 9.2 cm) are attached in these holders in such a way so that we can vary the pole gap. The Pole gap may vary from 0-10 cm. As the lower part of our cryostat has outer dimension 3.8 cm, pole gap of this size will be suitable for the magnet operation.
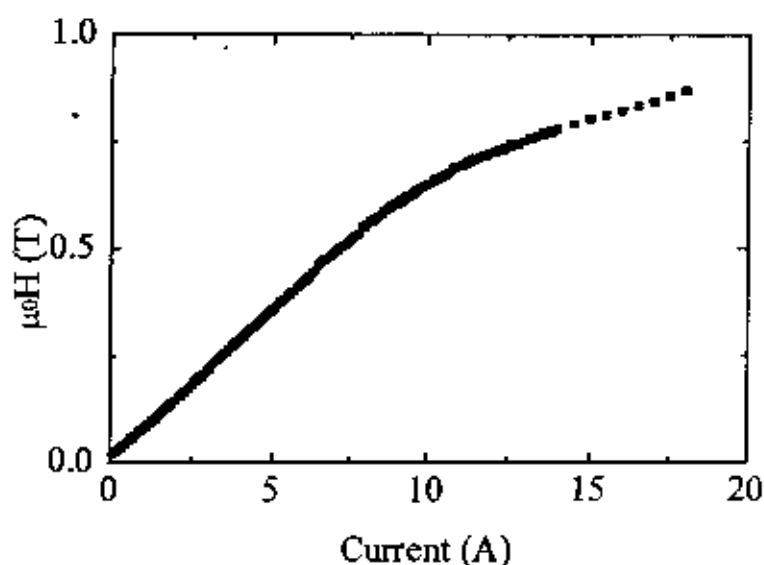
**Figure 3.3:** Calibration curve of the electromagnet.

Two induction coils for two pole-pieces have been made with insulated copper wire of No. S. W. G 14. The length of each of the coils is 12 cm. The number of turns in each layer of the coil is 58 and total number of layers is 44. So the total number of turns is 2552. The resistance of each coil is about 8 $\Omega$. The weight of each coil is about 40 Kg. Two coils are set in the pole pieces of the electromagnet. They are connected in parallel combination with the dc power supply. Calibration curve of the electromagnet is given in Figure 3.3.

### 3.4.3 Description of the sample rod

A sample rod is used for four-point resistance measurement. This is a hollow stainless steel tube. The upper part is connected with multi-pin connectors and lower part has a copper sample holder as shown in figure. The sample rod is connected with the cryostat by a union socket. A schematic diagram of the sample rod is shown in figure 3.4. This sample probe is used for four point resistance measurements. The temperature of the sample was measured using a thermocouple.
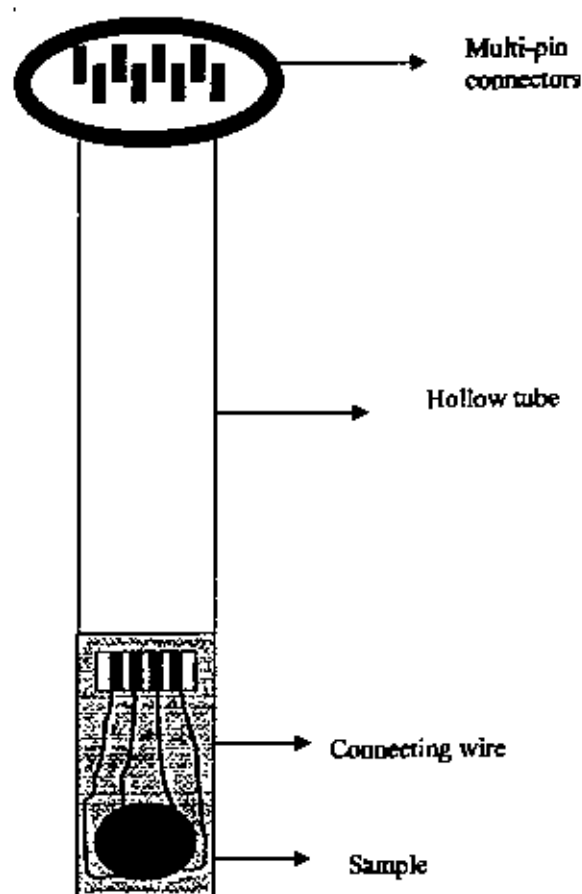
**Figure 3.4:** Schematic diagram of the sample holder.

## 3.5 Magnetoresistance Measurement Setup

Magnetoresistance measurements were carried out using the homely made cryostat and an electromagnet. Figure 3.5 shows the schematic diagram of the Magnetoresistance measurement.
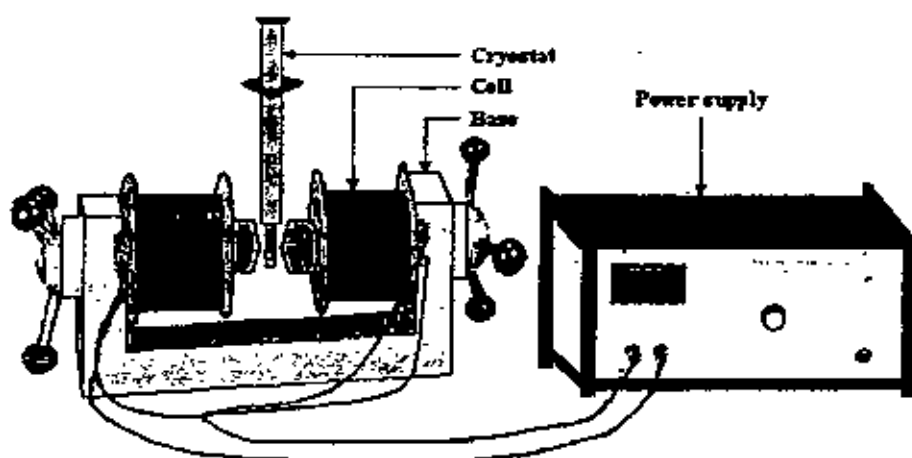
**Figure 3.5:** Schematic diagram of Magnet and Cryostat Assembly for Magnetoresistance Measurements.

The standard four point technique was used for resistance measurements. All samples for test are mounted on a probe and inserted in the sample well of the cryostat. The temperature of the sample is measured with a thermocouple placed close to the sample. A micro voltmeter was placed with the thermocouple to measure the voltage related to the temperature. The sample current is sourced with a constant current source and voltage drop is measure with micro voltmeter. For magnetoresistance measurements, the electromagnet is powered with a power supply. The system is capable of creating a field up to 0.86 T for a current of 18 A.

## 3.6 Lattice Planes and Bragg's Law

The peaks in an X-ray diffraction pattern are directly related to the atomic distance. Let us consider an incident X-ray beam interacting with the atoms arranged in a periodic manner as shown in figure 3.6. The atoms, represented as black sphere s in the graph, can be viewed as forming different sets of planes in the crystal (lines in graph on (a)).
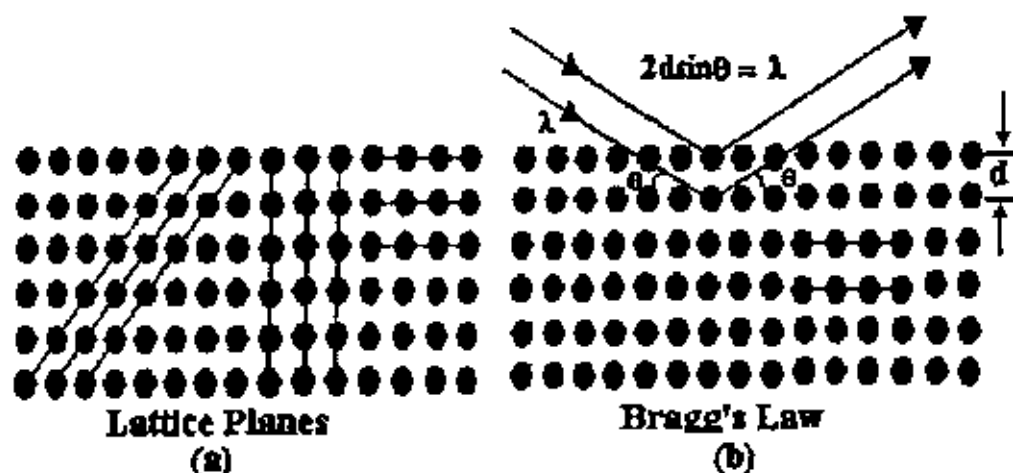


**Lattice Planes**
**(a)**

**Bragg's Law**
**(b)**

**Figure 3.6:** Bragg's law of diffraction (a) Different forms of lattice planes, (b) different from atoms.

For a given set of lattice plane with an inter- planner distance of d, the condition for a diffraction to occur can be simply written as lattice

$$2d_{hkl} \sin\theta = n\lambda$$

which is known as Bragg's law. Where, $\lambda$ is the wavelength of the X-ray $\theta$ is the scattering angle and n is an integer representing the order of the diffraction peak.

## 3.7 The van der pauw method

The van der pauw [1,2] method is based on four point probe measurement. This technique is use for the resistivity and Hall effect measurement. In essence it provides an easy way to measure sheet resistivity, Hall voltage and Hall mobility. The van der pauw technique can be used on thin sample of material and the 4 contacts can be placed anywhere on the perimeter/boundary, provided certain conditions are met as given below:

(i) The contacts should be on the circumference of the sample.

(ii) The contacts should be sufficiently small (as close as possible).

(iii) The sample is to be homogeneous and thin relative to the other dimensions

(iv) The surface of the sample is to be singly connected, i.e. the sample does not have isolated holes.

Figure 3.7 shows the four contacts on the circumference of the disc shaped sample. For a fixed temperature, we define resistance $R_{AB,\ CD}$ as the poteotial difference $V_D$-$V_C$ between the contacts D and C per unit current $I_{AB}$ through the contacts A and B. The current enters in the sample through the contact A and leaves it through B.
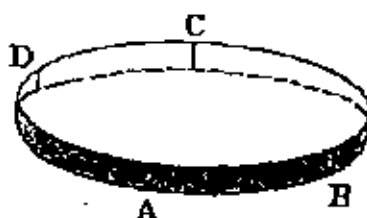


**Figure 3.7:** The four electrical contacts on the circumference of the disc shaped sample.

Then,
$$R_{AB,CD} = \frac{V_D - V_C}{i_{AB}} \qquad (3.1)$$

Analogously we define,
$$R_{BC,DA} = \frac{V_A - V_D}{i_{BC}} \qquad (3.2)$$

Van der Pauw method is based on the theorem that between $R_{AB,CD}$ and $R_{BC,DA}$ there exists the simple relation:

$$\exp\left(-\frac{\pi d}{\rho} R_{AB,CD}\right) + \exp\left(-\frac{\pi d}{\rho} R_{BC,DA}\right) = 1 \qquad (3.3)$$

Where d is the thickness of the uniform disc shaped sample and $\rho$ is the resistivity of the material. If d and the resistances $R_{AB,CD}$ and $R_{BC,DA}$ are known, then in Eq. 3.3, $\rho$ is the only unknown quantity.

In the general case, it is not possible to express $\rho$ explicitly in known functions. The solutions can, however, be written in the form

$$\rho(T) = \frac{\pi d}{\ln 2}\left(\frac{R_{AB,CD} + R_{BC,DA}}{2}\right) f\left(\frac{R_{AB,CD}}{R_{BC,DA}}\right) \tag{3.4}$$

where f is a function only of the ratio $R_{AB,CD}/R_{BC,DA}$ only and satisfies the relation

$$\cosh\left\{\frac{(R_{AB,CD}/R_{BC,DA}) - 1}{(R_{AB,CD}/R_{BC,DA}) + 1} \times \frac{\ln 2}{f}\right\} = \frac{1}{2}\exp\frac{\ln 2}{f} \tag{3.5}$$

Assuming $R_{AB,CD}/R_{BC,DA} = Q$, Eq.3.5 becomes,

$$\frac{Q-1}{Q+1} = \frac{f}{\ln 2}\operatorname{arccos}h\left\{\frac{\exp(\ln 2/f)}{2}\right\} \tag{3.6}$$

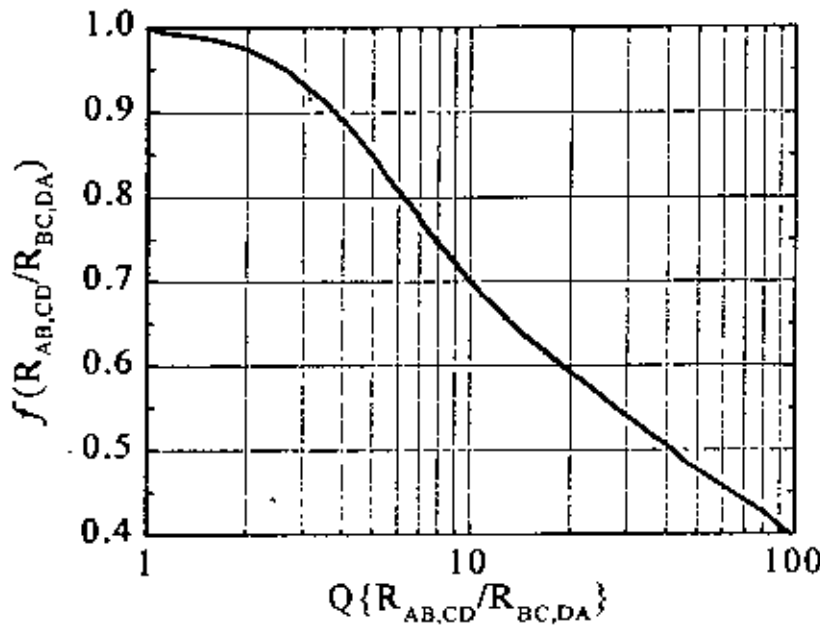A plot of this function is shown in figure 3.8.



Figure 3.8: The function $f(Q)$ for determining the resistivity of the sample.

In practice the electrical contacts have finite dimensions. van der Pauw showed that if one of the contacts is of finite length $l$ and is assumed that it lies along the circumference of the sample of diameter $D$ then

$$\frac{\Delta\rho}{\rho} \approx \frac{-l^2}{16D^2 \ln 2}.$$  (3.7)

Also, if all contacts have similar defects the errors introduced are additive. Our sintered disc shaped sample has a diameter ~11mm and if we assume the maximum width dimensions of the contacts are 1 mm then the errors introduced into our measurement due to finite sized contacts will be 0.3%. In fact, we have used 50 µm silver wire and conductive silver paint for the contacts which are much smaller than 1mm.

## References

[1]  van der Pauw L J, "A method of measuring specific resistivity and Hall effects of discs of arbitrary shape", Philips research reports, 13, 1 (1958).

[2]  van der Pauw L J, "A method of measuring specific resistivity and Hall    coefficient on lamellae of arbitrary shape", Philips technical review, 20, 220 (1958).

# CHAPTER 4

## Results and Discussion

The magnetoresistive properties of the polycrystalline bulk samples $La_{n-nx}Ca_{1+nx}Mn_{n-y}Cr_yO_{3n+1}$ ($x = 0.3$; $y = 0.075, 0.15, 0.3$; $n = 2, 3$) were studied. The DC electrical resistance measurements were measured from room temperature down to liquid nitrogen temperature both in zero field and in an applied magnetic field of 0.7 T. Magnetoresistance (MR) measurements were carried out and the MR behaviour was discussed as a function of magnetic field both at room temperature and at liquid nitrogen temperature. Activation energies for these polycrystalline samples were also calculated.

## 4.1    X-ray diffraction analysis

X-ray diffraction analysis was performed by powder X-ray diffraction (XRD) using Cu $K_\alpha$ radiation ($\lambda = 1.541$ Å) and Phillips (PW3040) X' Pert PRO X-ray diffractometer. The diffraction study indicated that the crystal structure of the bulk samples were of single phases with tetragonal perovskite structure having the lattice parameters a=0.3866 nm and c=1.8675 nm. Figure 4.1 shows the X-ray diffraction pattern for various sample $La_{n-nx}Ca_{1+nx}Mn_{n-y}Cr_yO_{3n+1}$ ($x = 0.3$; $y = 0.075, 0.15, 0.3$; $n = 2, 3$). Table 4.1 shows the comparative peak position (in angle) observed for the samples. The peaks in an X-ray diffraction pattern are directly related to the atomic distance. From the peaks in an X-ray diffraction pattern the inter- planner distance $d_{hkl}$ is measured using Bragg's law

$$d_{hkl}\sin\theta = n\lambda \qquad (1)$$

Where, $\lambda$ is the wavelength of the X-ray and $\theta$ is the scattering angle of the diffraction peak. From the X-ray diffraction patterns it was seen that all the samples showed the identical peak positions which confirmed the single-phase structure and homogeneity in chemical composition of the samples. Table 4.2 shows the lattice parameters for various samples.
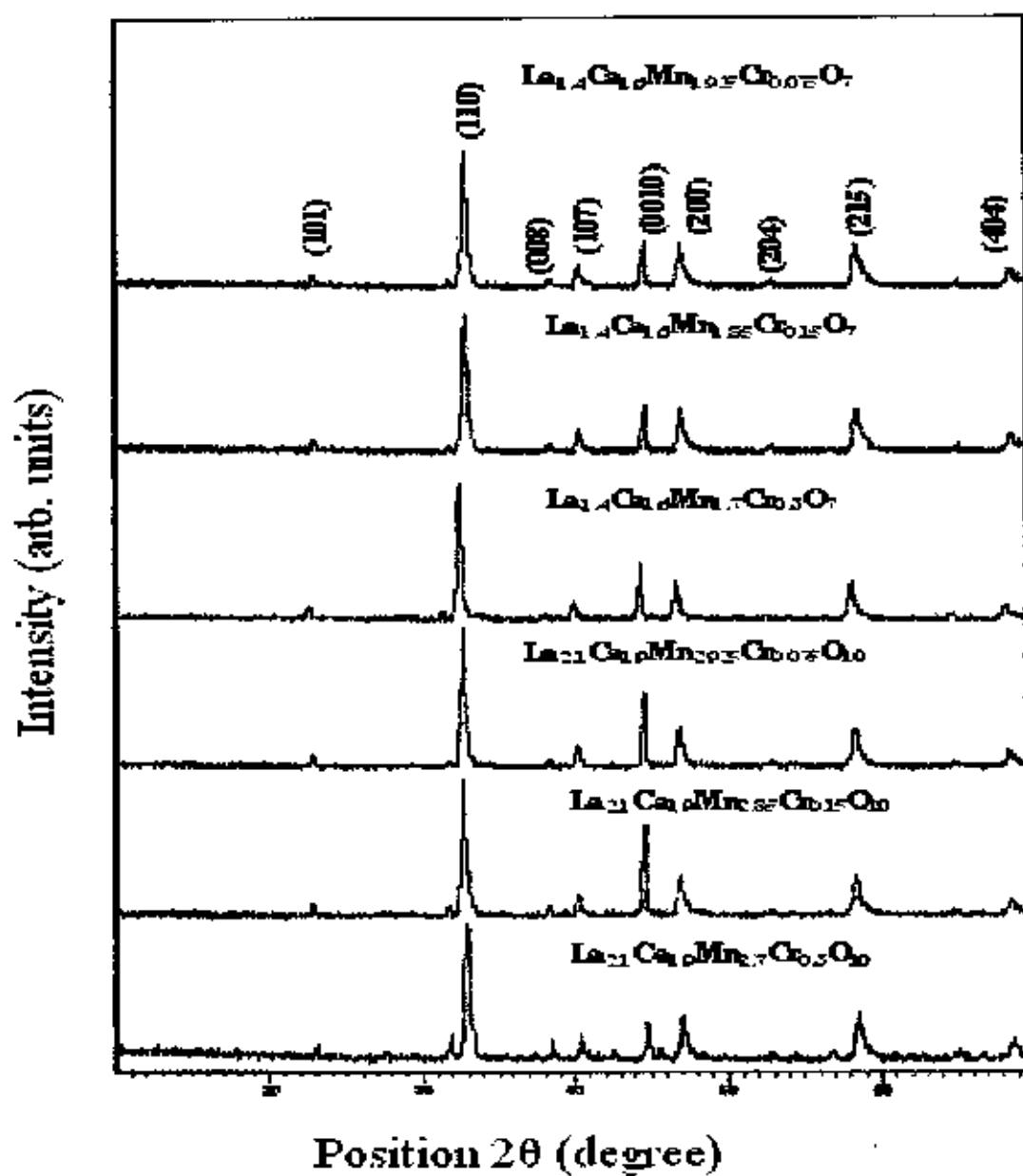
Figure 4.1: X-ray Diffraction patterns of polycrystalline bulk samples.

Table 4.1: X-ray diffraction peak positions for various polycrystalline samples

| Sample compositions | X-ray diffraction peak positions 2θ(degree) | | | | | | | | |
|---|---|---|---|---|---|---|---|---|---|
| | 1st | 2nd | 3rd | 4th | 5th | 6th | 7th | 8th | 9th |
| $La_{1.4}Ca_{1.6}Mn_{1.925}Cr_{0.075}O_7$ | 23 | 32.7 | 38.4 | 40.3 | 44.6 | 46.9 | 58.3 | 65 | 68.6 |
| $La_{1.4}Ca_{1.6}Mn_{1.85}Cr_{0.15}O_7$ | 23 | 32.7 | 38.5 | 40.4 | 44.7 | 46.9 | 58.4 | 65.1 | 68.6 |
| $La_{1.4}Ca_{1.6}Mn_{1.7}Cr_{0.3}O_7$ | 23 | 32.7 | 38.4 | 40.4 | 44.7 | 46.9 | 58.3 | | 68.6 |
| $La_{2.1}Ca_{1.9}Mn_{2.925}Cr_{0.075}O_{10}$ | 23 | 32.6 | 38.4 | 40.3 | 44.7 | 46.9 | 58.3 | 65.1 | 68.5 |
| $La_{2.1}Ca_{1.9}Mn_{2.85}Cr_{0.15}O_{10}$ | 23 | 32.7 | 38.4 | 40.4 | 44.6 | 46.9 | 58.4 | 65 | 68.5 |
| $La_{2.1}Ca_{1.9}Mn_{2.7}Cr_{0.3}O_{10}$ | 22.9 | 32.8 | 38.6 | 40.4 | 44.7 | 47 | 58.6 | 65.1 | 68.7 |

Table 4.2: Lattice parameters for various polycrystalline samples

:

| Sample compositions | a (nm) | c (nm) |
|---|---|---|
| $La_{1.4}Ca_{1.6}Mn_{1.925}Cr_{0.075}O_7$ | 0.386994 | 1.873921 |
| $La_{1.4}Ca_{1.6}Mn_{1.85}Cr_{0.15}O_7$ | 0.386856 | 1.868544 |
| $La_{1.4}Ca_{1.6}Mn_{1.7}Cr_{0.3}O_7$ | 0.386880 | 1.872321 |
| $La_{2.1}Ca_{1.9}Mn_{2.925}Cr_{0.075}O_{10}$ | 0.386961 | 1.871784 |
| $La_{2.1}Ca_{1.9}Mn_{2.85}Cr_{0.15}O_{10}$ | 0.387436 | 1.871784 |
| $La_{2.1}Ca_{1.9}Mn_{2.7}Cr_{0.3}O_{10}$ | 0.386364 | 1.865568 |

## 4.2    DC electrical resistivity

The normalized DC electrical resistivity for samples $La_{0-nx}Ca_{1+nx}Mn_{n-y}Cr_yO_{3n+1}$ ($x = 0.3$; $y = 0.075, 0.15, 0.3$; $n = 2, 3$) was measured by the standard four-point probe from room temperature down to liquid nitrogen temperature. The electrical resistivity was measured both in zero magnetic field and in presence of applied magnetic field (0.7 T). The applied magnetic field was perpendicular to the current flow in the sample.

The temperature dependence of normalized electrical resistivity of the Cr doped $La_{1.4}Ca_{1.6}Mn_{2-y}Cr_yO_7$ double layered perovskite manganites with different concentrations $y = 0.075, 0.15$ and $0.3$ at zero magnetic field and at the presence of 0.7 T magnetic field are shown in Figure 4.2.
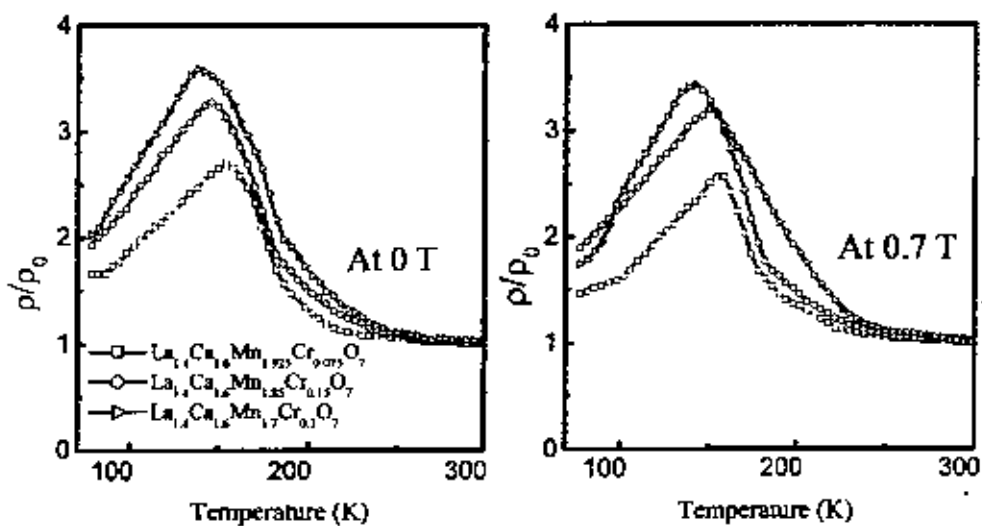


**Figure 4.2:** Normalized Resistivity as a function of temperature for $La_{1.4}Ca_{1.6}Cr_yMn_{2-y}O_7$ with $y = 0.075, 0.15$ and $0.3$ at 0 T and 0.7 T magnetic field.

From Figure 4.2 it is evident that, for all samples resistivity first increases with the decrease in temperature, and then exhibits peak around the metal-insulator (M-I) transition temperature denoted by $T_p$. For $T > T_p$, resistivity decreases with the increase of temperature. Concentrating on the behaviour of temperature dependent resistivity curve, it is noted that $d\rho/dT < 0$ for $T > T_p$, which is a characteristic of insulating behaviour. But for $T < T_p$, the sample showed metallic character with $d\rho/dT > 0$. It is also observed from

Figure 4.2, as Cr concentration increases, resistivity also increases but $T_p$ decreases. The M-I transition temperatures ($T_p$) defined by the temperature of the resistivity maximum are listed in table 4.3. At the presence of 0.7 T magnetic field it is also seen that all the samples show a metal insulator transition with a peak in the electrical resistivity when the temperature is decreased from room temperature. But the value of resistivity, in presence of magnetic field, decreases and the peak temperature $T_p$ shifts towards the high temperature region.

Figure 4.3 shows the variation of normalized resistivity as a function of temperature for triple layered perovskite samples $La_{2.1}Ca_{1.9}Mn_{3-y}Cr_yO_{10}$ with y= 0.075, 0.15 and 0.3 both at an applied magnetic field of 0T and 0.7T, respectively.
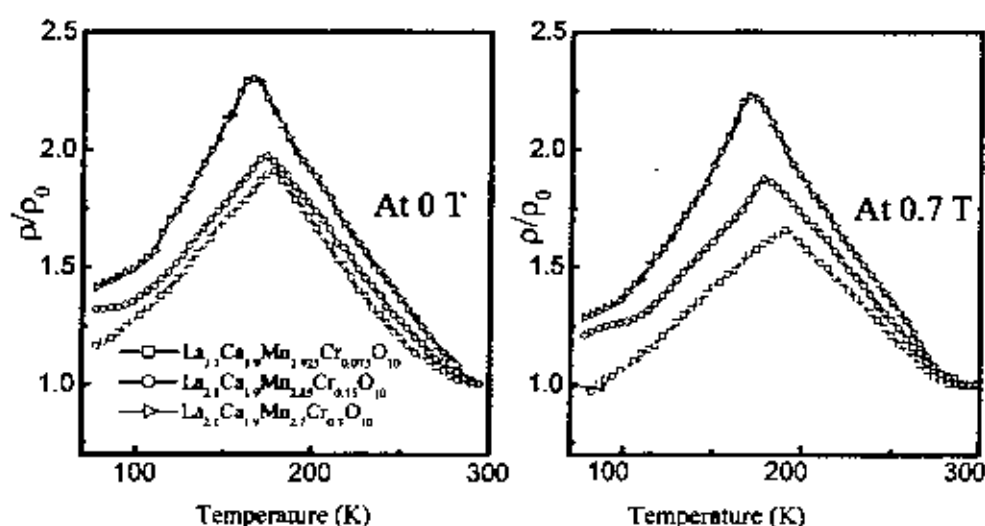


**Figure 4.3**: Normalized Resistivity as a function of temperature for $La_{2.1}Ca_{1.9}Cr_yMn_{3-y}O_{10}$ with y= 0.075, 0.15 and 0.3 at 0 T and 0.7 T magnetic field.

All the samples of $La_{2.1}Ca_{1.9}Cr_yMn_{3-y}O_{10}$ showed a metal insulator transition with a peak in the electrical resistivity around M-I transition temperature, $T_p$ like the previous double layered samples. Here also seen that with the increases of doping concentration the resistivity increases but M-I transition temperature, $T_p$ decreases. The value of resistivity

of the triple layered perovskite samples is lower than that of double layered samples, where the transition temperature shifts toward higher value for triple layer samples (Table 4.3).

The comparative study of temperature dependence of the normalized resistivity for various samples $La_{n-nx}Ca_{1+nx}Mn_{n-y}Cr_yO_{3n+1}$ (x=0.3, y=0.075), $La_{n-nx}Ca_{1+nx}Mn_{n-y}Cr_yO_{3n+1}$ (x=0.3, y=0.15) and $La_{n-nx}Ca_{1+nx}Mn_{n-y}Cr_yO_{3n+1}$ (x=0.3, y=0.3) for the values of n=2 and 3 both at 0 T and 0.7 T magnetic field are shown in figure 4.4, 4.5, 4.6 respectively. For all the samples it is observed that with the decreasing of $MnO_2$ layer from 3 to 2 the $T_p$ values decreases and the resistivity increases. This indicates that the transport and magnetic properties are sensitively dependent on the number of $MnO_2$ layers, n.
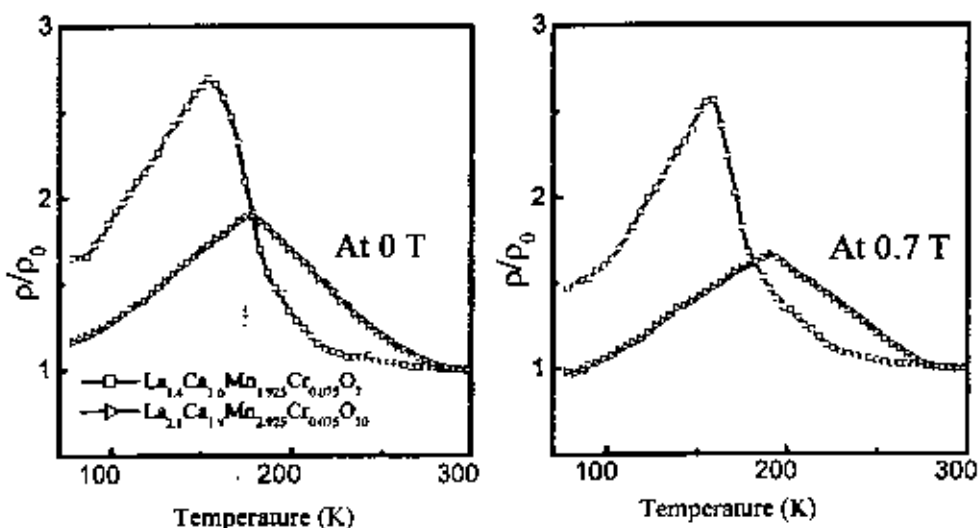


**Figure 4.4:** Normalized Resistivity as a function of temperature for $La_{n-nx}Ca_{1+nx}Mn_{n-y}Cr_yO_{3n+1}$ with x=0.3, y=0.075 both at the magnetic field 0T and 0.7T.
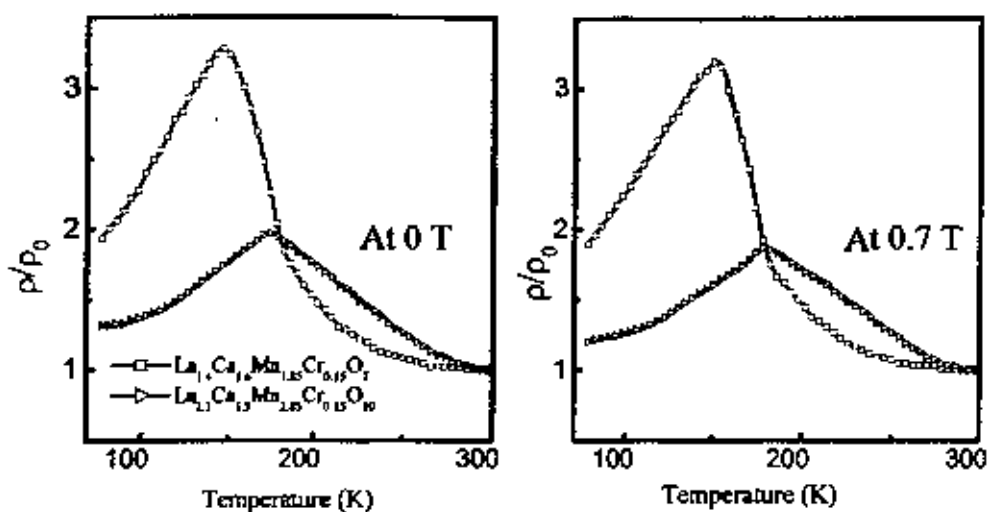
**Figure 4.5:** Normalized Resistivity as a function of temperature for $La_{0-0x}Ca_{1+0x}Mn_{0-y}Cr_yO_{3\sigma+1}$ with x=0.3, y=0.15 both at the magnetic field 0T and 0.7T.
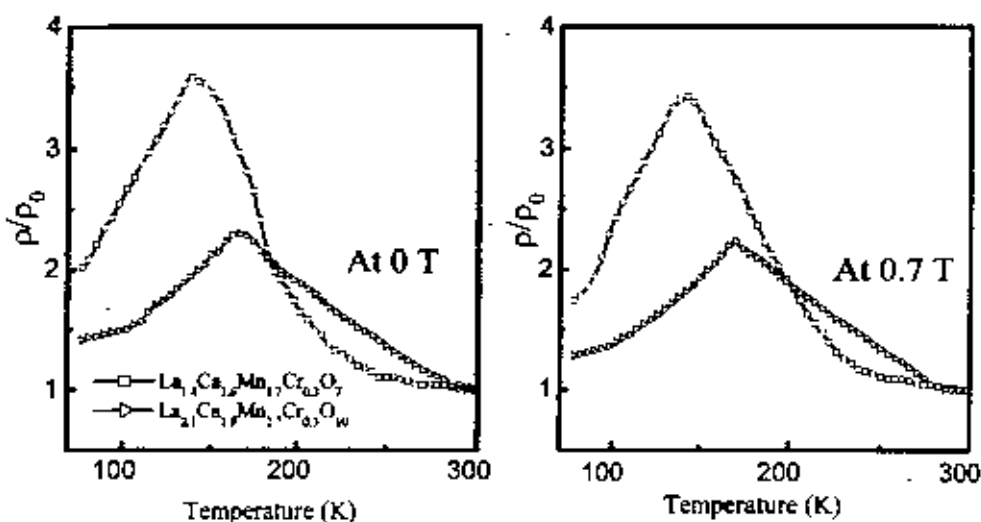


Figure 4.6: Normalized Resistivity as a function of temperature for $La_{0-0x}Ca_{1+0x}Mn_{0-y}Cr_yO_{5\sigma+1}$ with x=0.3, y=0.3 both at the magnetic field 0T and 0.7T.

**Table: 4.3** Transition temperature, $T_p$ and normalized resistivity at the magnetic field 0T and 0.7T.

| Sample compositions | $T_p$ at 0 T | $T_p$ at 0.7 T | $\rho/\rho_0$ at 0 T | $\rho/\rho_0$ at 0.7 T |
|---|---|---|---|---|
| $La_{1.4}Ca_{1.6}Mn_{1.925}Cr_{0.075}O_7$ | 154 | 157 | 2.69 | 2.57 |
| $La_{1.4}Ca_{1.6}Mn_{1.85}Cr_{0.15}O_7$ | 145 | 152 | 3.27 | 3.20 |
| $La_{1.4}Ca_{1.6}Mn_{1.7}Cr_{0.3}O_7$ | 138 | 143 | 3.58 | 3.42 |
| $La_{2.1}Ca_{1.9}Mn_{2.925}Cr_{0.075}O_{10}$ | 179 | 190 | 1.91 | 1.66 |
| $La_{2.1}Ca_{1.9}Mn_{2.85}Cr_{0.15}O_{10}$ | 173 | 178 | 1.97 | 1.87 |
| $La_{2.1}Ca_{1.9}Mn_{2.7}Cr_{0.3}O_{10}$ | 164 | 170 | 2.31 | 2.22 |

In order to explain the transport properties of the $LaMnO_3$-type system, electronic structure of the doping element must play a crucial role. In the present study it is observed that for all samples resistivity first increases with the decrease of temperature and display maximum resistivity at a respective temperature, $T_p$. After then resistivity decreases with the decrease of temperature i.e. it exhibit paramagnetic phase above $T_p$ and ferromagnetic phase below $T_p$. The parent compound, $LaMnO_3$, is a paramagnetic insulator (PMI) showing a phase transition to an anti-ferromagnetic (AFM) phase. With the Lanthanide (Ln) site doping by the alkaline earth metal, the hole doped oxide perovskites show the ferromagnetic metallic state below the Curie temperature $T_C$. The ferromagnetic metallic state in these compounds has been explained by the double exchange theory, which considers the transfer of an electron between $Mn^{3+}$-O-$Mn^{4+}$ ions [1]. As a result of strong Hund exchange coupling, the itinerant $e_g^1$ electrons (holes) interact with the localized $t_{2g}^3$ electrons ($S$=3/2), and thus mediate ferromagnetic ordering. In addition to the DE, a strong electron–phonon interaction giving rise to Jahn–Teller (JT) splitting of the outer $d$ level plays an important role in the transport mechanism, especially at temperatures near and above $T_p$. One way to monitor the DE interaction is by the substitution of divalent ions at the Ln site, leading to the variation of the ratio $Mn^{4+}/Mn^{3+}$ which might lead to the JT effect due to the change of $A$ site ion size. Another way is by doping of transition metal–ion at the Mn site, the center for the DE mechanism, which directly influences the DE interaction and hence the transport and magnetic properties.

In this investigation Cr is doped in Mn sites and these elements exist in the form of $Cr^{3+}$, $Mn^{3+}$, and $Mn^{4+}$. The present result in the DE framework suggests that $Cr^{3+}$ must be partly ferromagnetically coupled to the $Mn^{3+}$ and $Mn^{4+}$ species. The electronic configurations of these materials are $Cr^{3+}$: $t_{2g}^3$ (S=3/2), $Mn^{3+}$: $t_{2g}^3 e_g^1$ (S=2) and $Mn^{4+}$: $t_{2g}^3$ (S=3/2), among which only the $e_g^1$ electron of $Mn^{3+}$ is electronically active. The ionic radii of $Cr^{3+}$, $Mn^{3+}$, and $Mn^{4+}$ are 0.615, 0.645, 0.530 Å, respectively. Due to the nearly same ionic radius, the doped Cr ions replace $Mn^{3+}$ ions in the form of $Cr^{3+}$. $Cr^{3+}$ has the same electronic configuration ($t_{2g}^3$) as $Mn^{4+}$ and hence there should be FM double exchange interaction between $Mn^{3+}$ and $Cr^{3+}$ just as that between $Mn^{3+}$ and $Mn^{4+}$ [2,3]. It is evident that the presence of $Cr^{3+}$ in the $Mn^{3+}$–O– $Mn^{4+}$ network increase of electron–phonon interaction favoring the formation of polarons and hopping occurs between the different valence states of Mn in the insulating phase [4]. The nature of the charge carriers responsible for transport in such systems above $T_p$ is localized. On the other hand, in the low temperature phase, where ordering of the carriers takes place in the Mn network, favoring electron hopping from $Mn^{3+}$ to $Mn^{4+}$ sites leading to the FMM state due to double exchange. Hence with Cr doping in the La–Ca–Mn–O system, $Mn^{3+}/Mn^{4+}$ ratio decreases (as $Cr^{3+}$ acts as $Mn^{4+}$). But it is also known that $Cr^{3+}$– $Mn^{3+}$ FMDE interaction is smaller than that of $Mn^{3+}$– $Mn^{4+}$ [5]. Hence with Cr doping, the effective FMDE interaction becomes weaker, resulting in the gradual decrease of $T_p$ with increasing Cr concentration. Also due to weaker DE interaction, the only electronically active electron, $e_g^1$ electron of $Mn^{3+}$ ion, become localized [4,5] , causing the gradual increase in resistivity with increasing concentration.

In this investigation, it is also observed that the value of resistivity in presence of magnetic field (0.7 $T$) decreases but M-I transition temperature, $T_p$ shifts towards the higher temperature region. Cr substitution may also favor the charge carrier delocalization induced by the magnetic field, which suppresses the resistivity. The application of magnetic field enhances magnetic spin order and due to this ordering, the ferromagnetic metallic state suppresses the paramagnetic insulating state, which ultimately shift $T_p$ towards the higher temperature region.

The data listed in Table 4.3 indicate that the transport and magnetic properties are sensitively dependent on the number of $MnO_2$ layers, $n$. It is observed for each sample that with the decreasing of $n$ values transition temperature $T_p$ decrease and the resistivity increases. When a change from triple layered perovskites to double layered perovskites, there is a insertion of the insulating $(La,Ca)_2O_2$ layer into the perovskite layer [6-8]. This is expected to produce an anisotropic reduction of the one-electron $(e_g)$ bandwidth, which is the critical parameter governing the CMR and related properties in perovskite manganites. Theoretically, it is predicted that the $e_g$ bandwidth determines the transfer interaction between neighboring Mn sites. Within the framework of a simple double exchange theory, the exchange interaction is proportionally related to the transfer interaction, and the ferromagnetic transition is associated with the MI transition. Therefore, the MI and ferromagnetic transition temperature is expected to be proportional to the effective $e_g$ bandwidth $(W)$. The reduction in $W$ accompanied by a reduction in $n$ was also demonstrated in the magnitudes of the electrical resistivities. The increase in electrical resistivity $\rho$ with decreasing $n$ is attributed to a narrowing of the one-electron bandwidth. This is expected from the basic concept of the double exchange model, both $T_p$ and $\rho$ reflect real charge motion determined by the transfer interaction, via the one-electron bandwidth.

### 4.3 Magnetoresistance as a function of applied field

The magnetoresistance as a function of magnetic field for samples $La_{n-nx}Ca_{1+nx}Mn_{n-y}Cr_yO_{3n+1}$ ($x = 0.3$; $y = 0.075, 0.15, 0.3$; $n =2, 3$) were calculated at room temperature (300 $K$) and at liquid nitrogen temperature (78 $K$). Typical MR curves as a function of magnetic field obtained at room temperature are shown in figure 4.8. Room temperature MR was observed to be very low (~ 1-2%) and almost linear with field. A large value of MR is observed at 78 $K$ in the presence of low applied magnetic field. Hence it is clear that the degrees of spin polarization in these manganites are temperature dependent and increases with decreasing temperature just like $R_{1-x}A_xMnO_3$ manganites.

At low temperature (78 $K$) the strong linear field dependence of large $MR$ exists for a field of upto $H^*$ as shown in figure 4.9 & 4.10. The magnetic field $H^*$ designates the boundary of the two slopes. Beyond $H^*$ the magnetoresistance is a weak function of the applied magnetic field. We observed about 14%~30% MR at H*= 0.14T~0.21T. About 26% MR is observed at H*= 155mT for double layered $La_{1.4}Ca_{1.6}Mn_{1.925}Cr_{0.075}O_7$ sample and with the increase of Cr doping the percentage of MR is decreased. For the triple layered $La_{2.1}Ca_{1.9}Mn_{2.925}Cr_{0.075}O_{10}$ about 25% MR is observed at H*= 151mT and here also with the increase of Cr doping the percentage of MR is decreased. The total magnetoresistance of the double layered sample $La_{1.4}Ca_{1.6}Mn_{1.925}Cr_{0.075}O_7$ is 29% under the application of 860 mT magnetic field, where the triple layered $La_{2.1}Ca_{1.9}Mn_{2.925}Cr_{0.075}O_{10}$ sample show 26% MR under the application of 860 mT magnetic field. The value of $MR$ and corresponding $H^*$ for each sample at the liquid nitrogen temperature (78 $K$) are shown in Table 4.4. . It is observed from the table that with the increase of layer n, the percentage of MR is decreased.
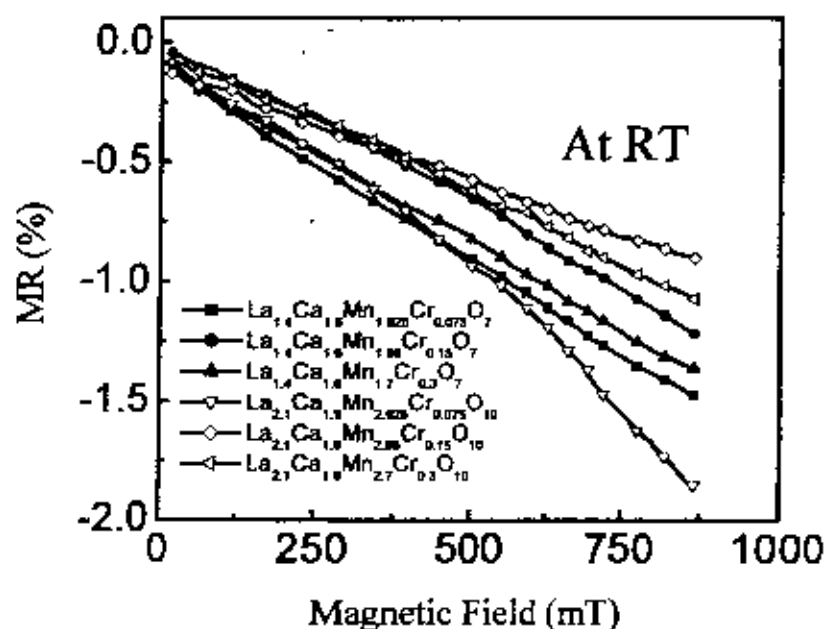


**Figure 4.7:** Magnetoresistance ($MR$) as a function of magnetic field at room temperature for various polycrystalline samples
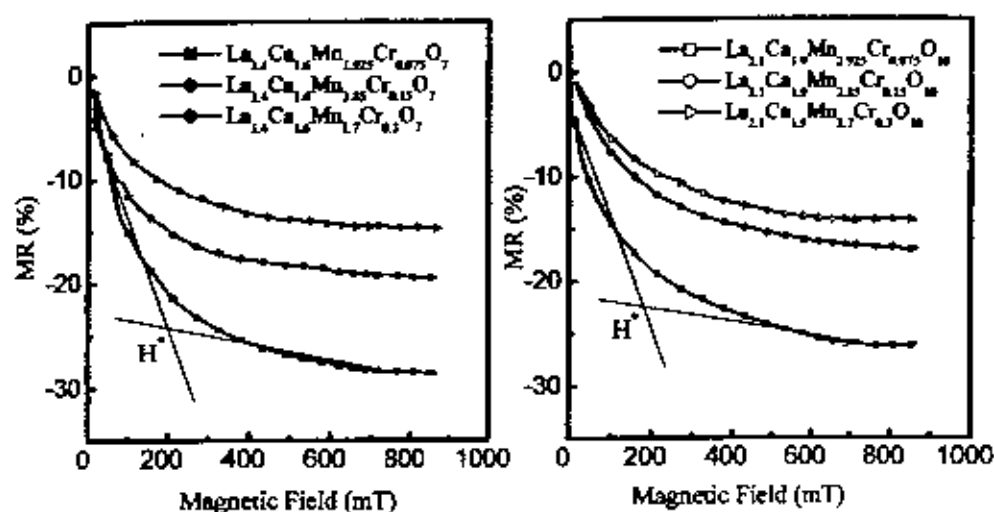
**Figure 4.8:** Magnetoresistance (*MR*) as a function of magnetic field at 78 K temperature for various polycrystalline samples $La_{1.4}Ca_{1.6}Cr_yMn_{2-y}O_7$ and $La_{2.1}Ca_{1.9}Cr_yMn_{3-y}O_{10}$

**Table 4.4:** Table for $H^*$, MR at $H^*$ and maximum MR at 78 $K$ for various polycrystalline materials

| Samples | $H^*$ (mT) | MR% | *Maximum MR%* |
|---|---|---|---|
| $La_{1.4}Ca_{1.6}Mn_{1.925}Cr_{0.075}O_7$ | 155 | 26 | 29 |
| $La_{1.4}Ca_{1.6}Mn_{1.85}Cr_{0.15}O_7$ | 143 | 17 | 19 |
| $La_{1.4}Ca_{1.6}Mn_{1.7}Cr_{0.3}O_7$ | 141 | 14 | 15 |
| $La_{2.1}Ca_{1.9}Mn_{2.925}Cr_{0.075}O_{10}$ | 151 | 25 | 26 |
| $La_{2.1}Ca_{1.9}Mn_{2.85}Cr_{0.15}O_{10}$ | 177 | 15 | 17 |
| $La_{2.1}Ca_{1.9}Mn_{2.7}Cr_{0.3}O_{10}$ | 208 | 13 | 14 |

The MR behaviour at room temperature for all samples found very low and is almost linear with field. At 78 K, a sharp increase of magnetoresistance was observed at low magnetic fields followed by a weak and linear dependence at high fields. The observed low temperature MR in these manganites can be attributed to grain and grain boundary effects, proposed by Akhter Hossain *et al*.[9]. According this model, the materials are subdivided into domains and low applied field is quite sufficient to align the domain spins and thus a sharp decrease in MR is observed. But to align the misaligned spins at the domain boundary region requires much larger field leading to weak field dependence. At T << Tc the material is in the ferromagnetic regime. In the absence of the field the magnetization of the grain of the polycrystalline material will be like that in fig. (a). The individual spins at the grain boundary region are randomly oriented. In the absence of the field, a carrier will suffer scattering from the unaligned magnetic domain, as well as disordered spin at the grain boundary region. By applying a low magnetic field, the magnetization of each grain starts to align towards the direction of the external magnetic field as fig. (b). However, a large magnetic field is required to align the spins of the grain boundaries.
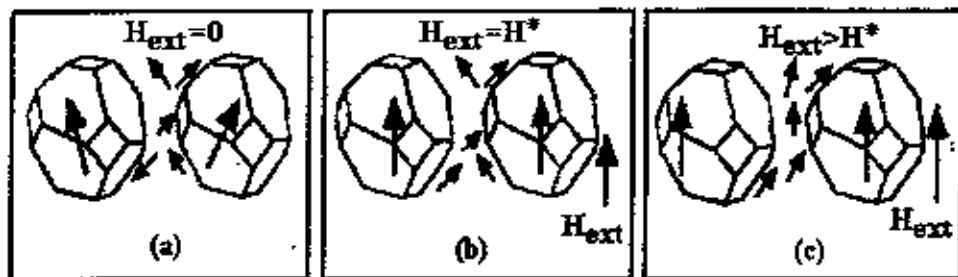


Figure 4.9: Schematic illustration of domain-boundary transport in a polycrystalline mixed-valence manganite proposed by Akhter Hossain *et al*. [9]

The other possible explanation of low field MR effect in these manganites is that when traveling across the grain boundary, conduction electrons may be subjected to a strong spin-dependent scattering. This scattering is reduced if a low external magnetic field can align the magnetizations of the neighboring grains. Spin alignment in the disordered surface layers in between the grains gives rise to high-field magnetoresistance.

## 4.5 Activation energy

The activation energy which explain the insulating-like behaviour of resistivity at temperature above $T_p$, can be calculated from the slopes of straight lines using the relation

$$\rho = \rho_0 \exp (E_0/K_B T) \qquad (1)$$

where, $E_0$ is the activation energy and $K_B$ is the Boltzman constant.

In fig. 4.19 ln $\rho/\rho_0$ is plotted as a function of $1/T$ for various divalent alkaline doped samples at both without magnetic field and with magnetic field. The temperature region is considered from transition temperature to room temperature. The values of activation energies for different samples are given in table 4.4.

From equation (4) the activation energy can be written as:

$$E_0 = [(\ln \rho/\rho_0)/(1/T)]K_B$$
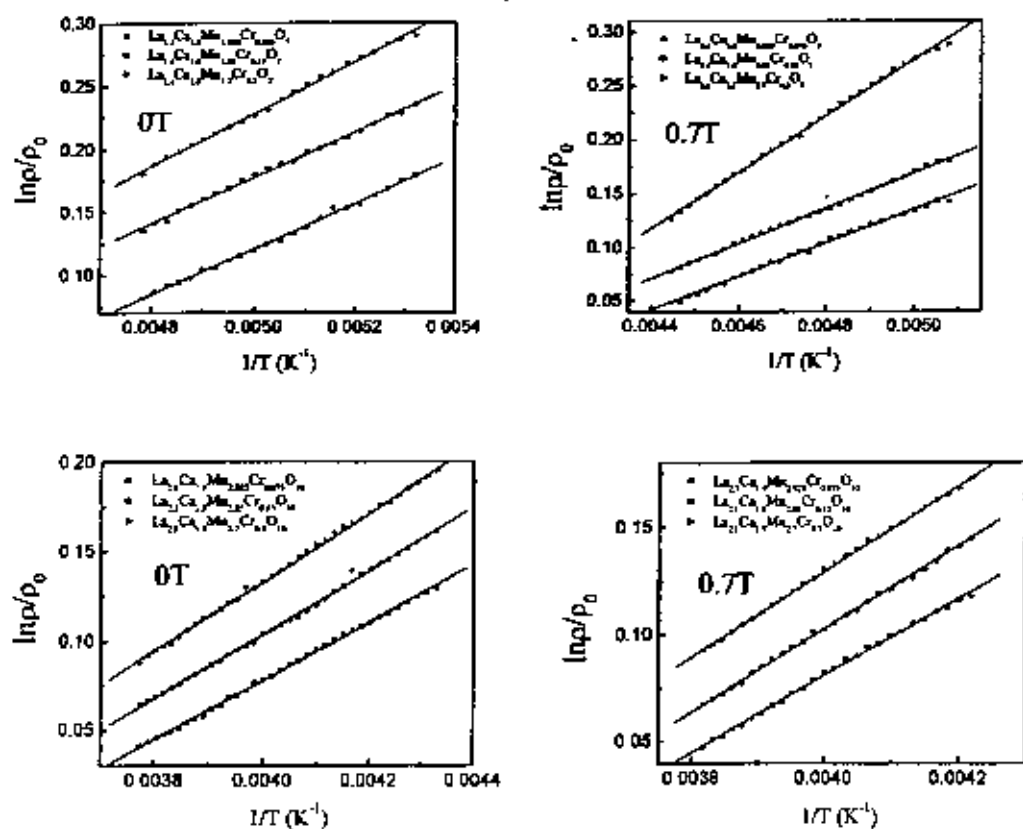$$= \text{slope} \times K_B$$

**Figure 4.10:** $\ln\rho/\rho_0$ is plotted against 1/T for various polycrystalline samples

**Table: 4.4** Activation energy (meV) of the polycrystalline samples.

| Samples | Activation energy (meV) (0T) | Activation energy (meV) (0.7T) |
|---|---|---|
| $La_{1.4}Ca_{1.6}Mn_{1.925}Cr_{0.075}O_7$ | 21 | 16 |
| $La_{1.4}Ca_{1.6}Mn_{1.85}Cr_{0.15}O_7$ | 29 | 23 |
| $La_{1.4}Ca_{1.6}Mn_{1.7}Cr_{0.3}O_7$ | 38 | 32 |
| $La_{2.1}Ca_{1.9}Mn_{2.925}Cr_{0.075}O_{10}$ | 16 | 13 |
| $La_{2.1}Ca_{1.9}Mn_{2.85}Cr_{0.15}O_{10}$ | 19 | 16 |
| $La_{2.1}Ca_{1.9}Mn_{2.7}Cr_{0.3}O_{10}$ | 26 | 24 |

All the samples show very good linear behaviour in the ln $\rho/\rho_0$ vs 1/T curve, which suggest that conduction occurs through a thermally activated process.

# References

[1] Zener C "Interaction between d shells in the transition metals", Phys. Rev. **81**,440 (1951).

[2] Banerjee A, Pal S, and Chaudhuri B K, "Nature of small polaron hopping conduction and the effect of Cr doping on the transport properties of rare earth manganites $La_{0.5}Pb_{0.5}Mn_{1-x}Cr_xO_3$", J chem. Phys, **115**(3), (2001).

[3] Vanitha P V, Santosh P N, Singh R S, RaoC N R, and Attfield J P, "Effect of cation size disorder on charge-ordering in rare earth manganites", Phys. Rev., **B59**, 13539 (1999).

[4] Maignan A, Caignaert V, Raveau B, Khomskii D, and Sawatzky G, "Thermoelectric Power of $HoBaCo_2O_{5.5}$: Possible Evidence of the Spin Blockade in Cobaltites", Phys. Rev. Lett. **93**, 026401 (2004)

[5] Zhang P L, and Zhang Y, Phy Rev B **61**, 8917 (2000).

[6] Cao X W, Fang J, and Li K B, "Electrical transport properties in magnetoresistive $La_{0.67}Ca_{0.33}MnO_3$ thin film", Solid State Communications, Volume **115** (4), 201-205 (2000).

[7] Asano H, Hayakawa J, and Matsui M, " Magnetotransport in perovskite series $La_{n-nx}Ca_{1+nx}Mn_nO_{3n+1}$ ferromagnets", Phys. Rev. B **57**(2) (1997).

[8] Fontcuberta J, Martinez B, Seffar A, Piñol S, García-Muñoz J L, and Obradors X, "Colossal Magnetoresistance of Ferromagnetic Manganites: Structural Tuning and Mechanisms",Phys.Rev.Lett.**76**,1122-1125(1996).

[9] Akther Hossain A K M, Cohen L F, Berenov A, Macmanus Driscoll J L, "Highly sensitive low temperature Low field colossal magnetoresistance in screen printed $La_{0.63}Y_{0.07}Ca_{0.30}MnO_3$ thick films" *Materials Science & Engineering B*, **83**(1-3), 79-83 (2001).
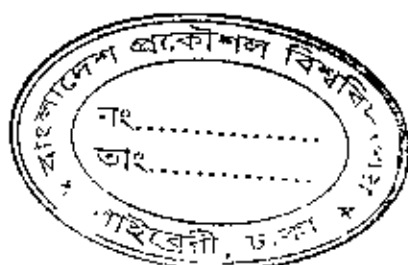
# Chapter-5

## Conclusions

The magnetoresistive properties of the polycrystalline samples $La_{n-nx}Ca_{1+nx}Mn_{n-y}Cr_yO_{3n+1}$ (x = 0.3; y = 0.075, 0.15, 0.3; n =2, 3) were investigated from room temperature down to liquid nitrogen temperature using standard four-probe technique at an applied magnetic field 0 T and 0.7 T. The structure and phase purity of the samples were checked by powder X-ray diffraction (XRD) using Cu $K_\alpha$ radiation by X-ray Diffractometer.

All the samples undergo a transition from an insulating to a metallic behaviour as the temperature is decreased from room temperature. The fundamental mechanism leading to the appearance of transport behaviour like metal-insulator transition in the present investigated samples was explained within the framework of Zener double exchange mechanism and Jahn-Teller lattice distortion.

Substitution of Cr in place of Mn created weaker $Cr^{3+}$– $Mn^{3+}$ ferromagnetic double exchange (FMDE) interaction than that of $Mn^{3+}$– $Mn^{4+}$. Hence with Cr doping, the effective FMDE interaction becomes weaker, resulting in the gradual decrease of $Tp$ with increasing Cr concentration. Also due to weaker interection, the only electronically active electron, $e_g^l$ electron of $Mn^{3+}$ ion, become localized, causing the gradual increase in resistivity with increasing concentration.

The resistivity vs temperature graphs with applied field in the same samples show similar behavior except the enhancement of M-I transition temperature by few Kelvin. This would be due to the suppression of spin fluctuations with the applied field in the paramagnetic region.

The MR behaviour at room temperature for all samples found very low and is almost linear with field. At 78 K, a sharp increase of magnetoresistance was observed at low magnetic fields followed by a weak and linear dependence at high fields. The observed low temperature MR in these manganites can be attributed to grain and grain boundary effects. The plot of ln $\rho/\rho_0$ vs $1/T$ suggest that conduction occurred through a thermally activated process above the transition temperature.